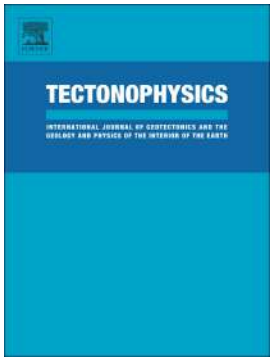

Reviewing megathrust slip behavior for recent Mw>8.0 earthquakes along the Peru-Chilean margin from satellite GOCE gravity field derivatives

Orlando Álvarez, Mario Gimenez, Andrés Folguera, Carlos Alberto Moreno Chaves, Carla Braitenberg

PII: S0040-1951(19)30295-1

DOI: https://doi.org/10.1016/j.tecto.2019.228188

Reference: TECTO 228188

To appear in: *Tectonophysics*

Received date: 20 February 2019

Revised date: 7 August 2019

Accepted date: 5 September 2019

Please cite this article as: O. Álvarez, M. Gimenez, A. Folguera, et al., Reviewing megathrust slip behavior for recent Mw>8.0 earthquakes along the Peru-Chilean margin from satellite GOCE gravity field derivatives, *Tectonophysics*(2019), https://doi.org/10.1016/j.tecto.2019.228188

Reviewing megathrust slip behavior for recent Mw>8.0 earthquakes along the Peru-Chilean margin from satellite GOCE gravity field derivatives

Orlando Álvarez[a,b,*] orlando_a_p@yahoo.com.ar, Mario Gimenez[a,b] gimmario@gmail.com, Andrés Folguera[c] andresfolguera2@yahoo.com.ar, Carlos Alberto Moreno Chaves[d] carlos.chavez@iag.usp.br, Carla Braitenberg[e] berg@units.it

[a]Instituto Geofísico y Sismológico Ing. Volponi, FCEFyN, Universidad Nacional de San Juan, Argentina.

[b]Consejo Nacional de Investigaciones Científicas y Técnicas, Argentina.

[c]INDEAN - Instituto de Estudios Andinos "Don Pablo Groeber". Departamento de Cs. Geológicas, FCEN, Universidad de Buenos Aires, Argentina.

[d]Instituto de Astronomia, Geofísica e Ciências Atmosféricas, Departamento de Geofísica, Universidade de São Paulo, São Paulo, Brasil.

[e]Dipartimento di Matematica e Geoscienze, Universita di Trieste, Via Weiss 1, 34100 Trieste, Italy.

ABSTRACT

The characterization of a seismogenic zone associated with the rupture process that occurs during great megathrust earthquakes has been approached from different perspectives. Different studies lightened the structural complexity and compositional heterogeneity of the interplate region. In this work, we address this relationship from the analysis of density contrasts provided by satellite gravity data and comparing these results with slip behavior along the rupture zone. We performed the calculation of gravity anomalies and gradients both corrected by the effect of topography and sediments. Then we analyzed this relation with the rupture zones of four megathrust earthquakes Mw>8 along the Peru-Chilean coast, associated with the largest earthquakes that occurred in the last years along this setting, finding that the maximum vertical displacements were located close to gravity minimums in the forearc zone. We finally obtained density models by inverting four trench-parallel profiles from the Gravity disturbance, finding low-density contrasts related to the maximum slips, and high density contrasts at its edges related to a decrease of the displacement or to the lateral ending of the rupture. The along-strike seismic segmentation observed previously in the gravity derivatives is also observed along dip, being slip increased at gravity lows and arrested at gravity highs, probably indicating that the forearc structure plays a key role in across strike rupture behavior in depth. Our results agree with the hypothesis that persistent tectonic features, modeled at a high degree by the oceanic plate morphology, may control strain accumulation and release along the megathrust.

Keywords: *Megathrust Earthquakes, GOCE, Rupture Area, Seismic Hazard, Chile, Subduction Zones.*

1. Introduction

The upper plate along active margins deforms to accommodate subducting relief and in response to stress transmitted across the plate interface and reactivation of previous basement anisotropies. Additionally, basin formation and magmatism that develops as a function of dehydration of the subducted slab at depth and decompression melting during extension produce a highly heterogeneous upper plate. This heterogeneous composition results in variations of rigidity across the continental margin (Basset and Watts, 2015a). Along more than 3,500 km, the Peru-Chilean margin is subject to high stress as a consequence of the oceanic Nazca plate subduction beneath the South American plate (e.g., Barazangi and Isacks, 1976; Jordan et al., 1983; Ramos and Folguera, 2009; Ramos, 2010; Horton, 2018). Although part of the deformation resulting from plate convergence is accommodated in an aseismic way, large earthquakes also occur, affecting hundreds of kilometers along coastal areas. In the last decade, three large earthquakes have affected the Chilean coast: the 2010 Maule Mw=8.8, the 2014 Pisagua Mw=8.2 and the 2015 Illapel Mw=8.3 earthquakes; while the most recent great megathrust earthquake that affected the Peruvian coast is the 2001 Arequipa Mw=8.4 earthquake (See. Fig.1).

Most studies show an anti-correlation between large earthquakes (Mw>8) and rough seafloor zones (aseismic ridges, plateaux, etc.), being these regions more favourable for the occurrence of many small earthquakes and creeping (Sparkes et al., 2010, Wang and Bilek 2011, 2014) and thus preventing for the nucleation of great megathrust earthquakes. Metois et al. (2016) found that five of six low coupling zones correlate with the subduction of high oceanic features that enter into subduction and all of them are associated with singularities in the coastline morphology often related to crustal fault networks. This low coupling areas behaved as barriers and stopped the ruptures, while coseismic asperities correlate well with highly coupled segments for the three most recent Mw>8 events along the Chilean margin. The asperities (Lay and Kanamori, 1981; Lay et al., 1982) are heterogeneities along the megathrust that concentrate high coseismic slip, high seismic moment release and high-stress drop, being most great megathrust earthquakes nucleated between 15-35km depth and promoting large rupture areas (Lay et al., 2012). Some asperities along central to southern Chile appear to have persisted over successive seismic cycles rupturing the same fault segment (such as happened in Japan, southern Alaska and Nankai), and appear to

correlate with persistent heterogeneities as sedimentary thickness or ocean roughness throughout the forearc and offshore regions. Along the Chilean coast, coseismic slip models, aftershocks and asperities are located seaward of the positive gravity derived anomalies, evidencing a direct relationship of these maxima and the downdip limit of seismogenic zone (Mendoza et al., 1994; Pritchard et al., 2007; Delouis et al., 2010; Loveless et al., 2010; Alvarez et al., 2014; Basset and Watts, 2015b).

Song and Simons (2003) and Wells et al. (2003) found that exists, statistically and at a global scale, a relationship between seismic asperities (characterized by high shear strength) along the megathrust with free air and trench parallel gravity lows, mostly coincident with the deep-sea terrace and forearc basins. One mechanism that could explain this relationship between basins centered asperities and seismogenesis is that basal erosion generates permanent forearc subsidence in the cases that the elastic deformation is not recovered during earthquakes (Sugiyama, 1994; Wells et al., 2003). In this model, trench-parallel variation in the forearc topography, gravity and seismogenic behavior is controlled by spatial variations in frictional properties of the plate interface. In contrast, Tassara (2010) proposed that the forearc density structure and related changes of vertical stress loading plays a key role on lateral variations of shear strength along the megathrust fault zone for the Chilean margin. Recently the higher resolution of GOCE data allowed mapping with greater detail the relationship between along strike density changes and historic rupture zones along the Chilean margin (Alvarez et al. 2014), a ratio that improves as the event magnitude increases (Alvarez et al., 2015a).

Bilek and Lay (1999, 2002), Bilek (2007) and Lay and Bilek (2007) largely studied depth varying rupture attributes and general spatial heterogeneity and more recently Lay et al. (2012) introduced depth varying domains (A, B C, D) with distinct seismic radiation characteristics focused on the along-dip variation of short period energy release (See Fig. 1). They found strong tsunami excitation at shallow depths from 5 to ~18 km (domain A) where there is very little high-frequency seismic radiation. Large and relatively uniform regions with unstable sliding frictional properties (asperities) generate modest levels of diffuse short-period radiation and large slip from the central domain B (at source depths spanning from 15 to 30 km) where most megathrust events occur. In this model, the down-dip part of the megathrust may be enriched in patchy, isolated smaller-scale asperities

surrounded by "aseismic" conditionally stable areas, which would produce concentrated bursts of short-period radiation during domain C events (at depths between 30-50km) that accentuate strong ground shaking hazard from the deeper ruptures (Ye et al., 2016a, b). The last domain (D) represents a transition at the deep edge of the seismogenic zone and is only present in some regions, with diverse observations of slow slip events, low-frequency earthquakes and/or sesimic tremor.

These distinct domains serve as a general framework for considering hazards for great megathrust earthquakes (Ye et al., 2016). Mapping these heterogeneities (along and across-strike) is a formidable task that just started to develop, being approached from different methodologies and databases. Since satellite GOCE mission beginning, a possible contribution of GOCE derived gravity gradients to the improvement of interpretation of large earthquakes was expected, and this is being achieved. Due to its improved spatial resolution and homogeneous data quality, lateral variations in crustal and lithospheric thickness can be studied (i.e. Earth structure), to discriminate between linear and non-linear rheologies (i.e. Earth rheology) and also contribute to improving our knowledge of the mechanisms of stress accumulation and stress release (Bouman et al., 2012). Mapping along-strike and along-dip variations of the density structure over the seismogenic zone could serve as a proxy to study the distinct behavior of asperities and barriers during rupture propagation. In this work, we investigate a possible relationship between GOCE gravity field derivatives and slip patterns for the last Mw>8 earthquakes along the Chilean margin, to find a potential tool to characterize the megathrust to anticipate future margin behavior during rupture propagation.

Figure 1

2. Methodology

Satellite-derived gravity data have the surpassing advantage of being able to map the whole megathrust zone without the limitations that currently condition (except for a few exceptions as seafloor geodesy) the terrestrial measurement systems (e.g. GPS, seismological stations) and also other satellite systems which only provide useful data on the earth's surface (InSar). Following Kopp (2013) who claims that it is imperative to 'overcome the shoreline' in data analysis, a technologically induced obstacle that separated

geophysical studies into offshore and offshore domains. Exploiting this comparative advantage we performed a detailed gravity analysis using direct and inverse models, to unravel the density structure along the megathrust both along and across-dip to be compared to slip patterns for the last Mw>8 earthquakes along the Chilean margin.

2.1. Satellite GOCE derived gravity data

The disturbing potential (T) is derived (Janak and Sprlak, 2006) by subtracting the normal potential field of the reference ellipsoid (WGS84) from the observed potential. The last satellite GOCE model GO_CONS_GCF_2_DIR_R5 (Bruinsma, 2013) is a full combination of GOCE-SGG (Satellite Gravity Gradiometer), GOCE-SST (Satellite-to-Satellite Tracking), GRACE (Gravity Recovery and Climatic Experiment) and LAGEOS (Laser GEOdynamics Satellite). This satellite-only model obtained by the direct approach method leads to an excellent performance of the long as well as of the short wavelengths when compared to previous GOCE models (processing details are given in Pail et al., 2011 and Bruinsma et al., 2010). One outstanding characteristic is that presents homogeneous precision and it is presently the one of maximum degree/order (N=300) from satellite-only data up, being the half-wavelength resolution of approximately 67 km according to $\lambda/2=\pi R/Nmax$ (Li, 2001; Hofmann-Wellenhof and Moritz, 2006; Barthelmes, 2013) with R being the mean Earth radius and Nmax the maximum degree/order of the harmonic expansion.

By direct modeling of the satellite-only GOCE data, from the spherical harmonic coefficients (Janak and Sprlak, 2006) on a regular grid of 0.05º grid cell size, we obtained the gravity disturbance and the vertical gravity gradient. The gravity disturbance (Gd) is calculated by subtracting the effect of the reference potential from the observed gravity over the ellipsoid (Barthelmes, 2013). Then it was reduced by the topographic effect to highlight the different density contrasts inside the crust (Hofmann-Wellenhof and Moritz, 2006; Molodensky, 1945; Molodensky, et al., 1962):

$$Gd = \delta_{g_{tr}}(h,\lambda,\phi) = g_{obs}(h,\lambda,\phi) - \gamma(h,\phi) - g_t(h,\lambda,\phi)\ [\mathbf{mGal}] \qquad \textbf{Ec. 1}$$

where g_{obs} is the observed gravity, g_t is the effect of the topographic masses over ellipsoid and γ is the gravity of the reference potential.

The vertical gravity gradient (*Tzz*) is obtained as the second radial derivative of the disturbing potential (Tscherning, 1976; Rummel et al., 2011):

$$T_{zz} = \frac{\partial^2 T}{\partial r^2} \left[\mathbf{1\ Eötvös} = \mathbf{10^{-4}\,\frac{mGal}{m}}\right] \quad \mathbf{Ec.\,2}$$

The Tzz is expressed in Eötvös and represents a better theoretical resolution than the gravity vector itself for detecting crustal density variations (Li, 2001) (mainly shallower structures with high-density contrast), allowing determining the edges of anomalous masses with better detail and accuracy. The gravity disturbance presents a spread signal highlighting deeper sources (Braitenberg et al., 2011). Although both quantities are slightly different for the same structures, they behave in a complementary way. This methodology has already been used in Alvarez et al. (2014, 2015a; 2017a, b; 2018a) and also in Spagnotto et al. (2018) for studying great megathrust earthquakes, with a detailed description presented in Alvarez et al. (2012, 2013).

2.2. Reduction by topographic and sediments effect

To eliminate the correlation of the gravity signal with the topography, the topographic effect must be removed from the satellite observations (Forsberg and Tscherning, 1997). The effect generated by the topographic masses on the gravity field and over its derivatives is calculated following Newton's law of universal gravitation. To remove the topographic effect from Gd and Tzz, we calculated the topographic contribution by discretizing a global relief model which includes ocean bathymetry (ETOPO1, Amante and Eakins, 2009) using spherical prisms of constant density (Heck and Seitz, 2007; Wild-Pfeiffer, 2008; Grombein et al., 2010, 2013).

By taking into account a spherical approximation (instead of a planar one), we considered the Earth's curvature (Uieda et al., 2010, 2016), avoiding considerable errors as the region under study is wide (Hofmann-Wellenhof and Moritz, 2006; Alvarez et al., 2012, 2013; Grombein et al., 2013, Bouman et al., 2013). We performed the calculation of the topography contribution over Gd and Tzz using the software Tesseroids (Uieda et al., 2010; Alvarez et al., 2013), densities used are mean standard values for topographic density reduction: 2.67 g/cm3 for masses above sea level and 1.03 g/cm3 for seawater (e.g. Ebbing et al., 2007, Braitenberg, 2014). The calculation height is of 7,000 m to ensure that all values are above the topography. For the vertical gravity gradient, the topographic

reduction amounts up to tens of Eötvös, and up to a few hundreds of mGal for gravity. The topographic effect was filtered by using a 4th order Butterworth filter at 133km wavelength to compare to satellite data at comparable wavelengths.

The sediment reduction was performed using the same method considering a mean density of 2.4 g/cm3. This sediment density were used in the region by Ranero et al. (2006) and obtained from modeling wide-angle seismic and gravity data (Sallares and Ranero, 2005). Sediment thicknesses were obtained from the National Geophysical Data Center - NOAA (NGDC's) global ocean sediment thickness grid (Whittaker et al., 2013), an updated version of the NGDC's original ocean sediment thickness grid from Divins (2003). The sediment correction reaches up to 1.5 Eötvös to the south of JFR where sediment thickness is higher (more than 1km and increasing to higher latitudes), in this region, the sediment gravity effect has enough impact to be removed to solve buried structures. Over the region of the Illapel earthquake the reduction reaches between 1 and 1.5 Eötvös, and decreases to the north were the Chilean trench is almost starved of sediments (< 500m) (e.g. Lamb and Davis 2003, Völker et al., 2006).

2.3. Tzz harmonic decomposition from spherical coefficients

Featherstone (1997) performed a spectral analysis of the geoid and gravity anomalies and found that by cutting-off the degree/order of the harmonic expansion allows decomposing the gravimetric signal as causative mass depth increases. In recent work (Alvarez et al., 2017a), we derived an equation (Ec. 1) relating the depth (Z_l) of a causative mass with a determined degree of the spherical harmonic expansion (N) for the Tzz, based on the last author.

$$Z_l = \frac{(R_E + H_c)(N-1)}{(N+2)(N+1)} \quad \textbf{Ec. 3}$$

Where R_E =6,371 km is the Earth's radius, H_C is the ***Tzz*** calculation height and N is the degree/order of the harmonic expansion. Table 1 shows for different degree/orders the corresponding depth Z_l and spatial resolution. Higher orders are associated with shallower sources (low Z_l), while low orders are related to deeper mass anomalies (higher Z_l).

Results from this harmonic decomposition tool by truncating the harmonic expansion allow analyzing Tzz response with increasing depths of the causative masses for the different events under study.

Table 1

2.4. Inversion model from the residual gravity disturbance (Gd)

We performed 2D inverse gravity modeling (see Spagnotto et al. 2018) from the topography and sediment corrected residual gravity disturbance (Gd) along different trench parallel sections over main ruptures along the Peruvian-Chilean trench. The inverse problem theory objective is to determine the model parameters $\hat{\boldsymbol{\rho}}$, from the observations g_{obs}, such as predicted data $\hat{g} = f_{(\hat{\rho})}$, minimizes the distance $g_{obs} - f_{(\hat{\rho})}$. For the estimation of the 2D density distribution model, the study region was divided into blocks of rectangular prisms. The density model is adjusted through successive iterations until the signal generated fits with the observed data by using a 2-D inversion algorithm from Chaves and Ussami (2013). This algorithm is based on the minimum norm problem solved by the method of Lagrange multipliers following Boulanger and Chouteau (2001). As it is possible to find more than one set of parameters that precisely fit the observations, a priori known information (Menke, 1984) is needed to solve undetermined problems and to constrain the solution better.

The algorithm solves the inversion problem by iteratively calculating the parameters of the model, such as density, considering a series of constraints such as minimum distance, flatness, smoothness and compactness, which are combined using a Lagrange function (Boulanger y Chouteau, 2001). Different "weights" were assigned to each block depending on its depth, a priori information of the density and its range of possible variation for the region under study was also considered. The recovery of the geometry (depth and size) and the distribution of densities of the original model are dependent on the set of constraints used.

The resulting 2D model represents a possible distribution of densities contrasts that responds to the observed signal, taking into account many restrictions (e.g. depth of the model, range of density variation, block size, cells depth-depending weighting, and minimum volume) and the maximum error considered. Even though the solution that

satisfies the observed data can be obtained quickly, the non-uniqueness in the potential methods is due to the nature of the physics and low-determination of the problem (Boulanger and Chouteau, 2001).

First, we calculated the gravity disturbance from the satellite GOCE model GO_CONS_GCF_2_DIR_R5 (Bruinsma, 2013) (on a regular grid with a cell size of 0.05º) up to degree/order N=300. The gravity disturbance was calculated after subtracting the gravity field of the reference ellipsoid (WGS84) from the observed gravity of GO_CONS_GCF_2_DIR_R5 model (Janak and Sprlak, 2006). Then we computed a residual Gd by subtracting the same model but developed up to degree/order N=10, and thus removing deeper sources and regional effects. Finally, we removed the topographic effect and the effect of sedimentary thickness by using the global relief model ETOPO1 (Amante and Eakins, 2009) with a standard density of 2,670 kg/m^3 and using sediment thickness from CRUST1.0 (Laske et al., 2013) with a standard density of 2,400 kg/m^3 respectively (Uieda et al., 2017).

For the construction of the 2D models, the study region was subdivided into rectangular cells (see Table 2). The estimated density model uses a starting model with density contrast equal to zero. The modeled density distribution is adjusted through successive iterations, until the signal generated fits with the observed data, considering a value of root mean square error of 0.1 (Chaves and Ussami, 2013). Other acceptance criterions for convergence of the solution were also considered as the ratio between $\frac{\Delta\hat{\rho}_i}{\hat{\rho}_i} < 0.01$ were $\hat{\rho}$ are the iteratively esteemed model parameters obtained as $\hat{\rho}_{i+1} = \hat{\rho}_i + \Delta\hat{\rho}_i$ (see Chaves and Ussami, 2013 for a detailed description). The inversion may also be stopped after 450 iterations.

In order to improve the resolution of the inverse method this program implements some constraints comprised in the sensitivity matrix **G** (g=Gρ in a matrix notation) that relates the gravimetric acceleration ***g*** (data) and the contrast of density ***ρ*** (parameters), making data less dependent on the specific parameters of observations by giving different weights to them (Zhdanov 2002). A hard constraint is based on a priori known density variation range $\rho_{min} \leq \rho_j \leq \rho_{max}$, for which we considered density ranges indicated in Table 2 for each case. Another constraint is the depth-weighting matrix Q (Li and Oldenburg 1996, 1998; Pilkington, 1997), which gives the same probability to each block during the inversion

process (Chavez and Ussami, 2013). By weighting cells with an inverse function of depth (z), such as $\frac{1}{(z_i+\varepsilon)^B}$, this is a method to counteract cell's sensitivity decrease with depth avoiding a shallow density concentration in the solution, being ε a small number to avoid singularity at the surface (Boulanger and Chouteau, 2001). Boulanger and Chouteau (2001) performed many tests and found that the best value of B is equal to 0.9 and an acceptable range is [0.5, 1]. Chavez and Ussami (2013) also selected this value based on the best fit of the data and the ability of the inversion algorithm in estimating a density model close to the synthetic one. After many tests, we selected a B factor for each profile, as indicated in Table 2, to control the weight of Q on the matrix G. A minimum volume constraint matrix V modified by Boulanger and Chouteau (2001) from Last and Kubik (1983) is used to concentrate the solution in a minimum volume by decreasing the amplitude of density contrast ρ_j. Table 2 also shows the number of iterations, the RMS error and the ratio reduction for each profile.

Table 2

3. Analysis of seismotectonics from satellite gravity data

Four major earthquakes with Mw>8.0 stroke the Peru-Chile margin in the last two decades. These events have been extensively analyzed from different datasets, with wide seismic and GPS networks along the margin, resulting in well-constrained slip models. In this work, we compared our results with the slip models for these events, analyzing the rupture propagation pattern and its relation with the distribution of mass heterogeneities from GOCE data.

3.1. The Arequipa Mw=8.4 earthquake

The June 23, Mw = 8.4 Arequipa earthquake in 2001 (16.265°S 73.641°W at ranging depth between 22km to 33 km as reported by Ruegg et al., 2001; Kikuchi and Yamanaka, 2001; Giovanni et al., 2002; USGS; among others) reactivated the northern portion of the 1868 rupture, leaving the southern segment unbroken. This underthrusting event has an aftershock area of 320 km by 100 km approximately (Giovanni et al., 2002). The 2001 Arequipa event Mw = 8.4 and its Mw = 7.6 aftershock (July 7, 2001) seem to have released less than 50% of the moment that was released during the great 1868 Mw8.8 earthquake

(Nishenko, 1985; Dorbath et al., 1990; Comnte and Pardo, 1991). Analyzing the source time functions for the 1974 (M0 = 8.0), 1996 (MW = 7.7), 1942 (MW = 7.9–8.2), and 2001 (Mw 8.2) earthquakes along the southern Peru trench (Beck and Ruff, 1989; Swenson and Beck, 1999, 1996), Giovanni et al. (2002) found that although there is some overlap along strike in their aftershock areas there seems to be no overlap in the rupture of the largest asperities associated with each event. The last authors observed that the regions of higher moment release for these events are small compared to the entire fault area as defined by the aftershocks.

Figure 2

3.1.1. Results:

3.1.1.1. Earthquake rupture behavior from Tzz

The expression of the Nazca Fz cutting across the forebulge (Fig. 2A) is clearly depicted by a segmentation of the gradient signal separating a domain of higher Tzz values (>+25 Eötvös) from lower values to the south (up to +20 Eötvös). The extrapolation of this Fz path under the forearc, following the convergence direction (DeMets, 2010), coincides with a Tzz minima lobe (<-15 Eötvös). Basset and Watts (2015a) reported that subducting Fz. residual gravimetric expression extends >200 km landward of the trench axis.

In a general analysis, there is a good spatial correlation along strike between low ***Tzz*** signal and high seismic slip over the marine forearc (Fig. 2A). This relationship was also addressed in a previous work by Alvarez et al. (2015a) who related minimum Tzz (<0 Eötvös) to highly coupled regions that acted as seismic asperities mainly associated with subducted sediments and forearc basins. The harmonic decomposition of the Tzz (that allows mapping different mass heterogeneities along dip, see Fig. 3) shows a negative anomaly which continues in-depth, as shown by de inversion model (section 3.1.1.4). To the north and NE of the main rupture following the coastline, a local positive (> +15Eötvös) is unraveled coincident with the down dip ending of the rupture (Figs. 2 and 3).

3.1.1.2. Southern directivity and main asperity from Tzz

Previous studies (Bilek and Ruff 2002; Giovanni et al., 2002; Audin et al., 2008) show that the rupture propagated unilaterally to the southeast over 300 km, presenting the second larger pulse of moment release at 120-130 km of the mainshock in this direction (centered

at approximately 17ºS 73W between the two main clusters of aftershocks); and stopped near the Ilo Peninsula. Giovanni et al. (2002) identified two regions of higher moment release (asperities) from the source-time functions, a first peak corresponding to a smaller asperity close to the hypocenter and a second larger peak that corresponds to the larger asperity containing more than 2/3 of the total moment release from the body waves. Strong unilateral rupture directivity to the southeast is also suggested by surface wave data (Bilek and Ruff, 2002). Different teleseismic-only models coincide in the location of largest moment release about 120 km southeast of the hypocenter (the main asperity), with a few other regions of significant moment release/enhanced slip (Kikuchi and Yamanaka, 2001; Bilek and Ruff, 2002). There are also two pulses in the GPS inversion (Norabuena, 2004), but Pritchard et al. (2007) found that a single station almost completely controls the slip distribution in this area. Comparing seismic and geodetic inversions, Pritchard et al (2007) found that slip from the InSAR-only model is more continuous between the hypocenter and the main asperity and that slip in the geodetic-only models is mostly located about 20 km deep, while there are two peaks in the teleseismic slip at about 60 km and 15 km depth respectively.

The epicenter for de Arequipa earthquake nucleated close to a high Tzz anomaly (Figs. 2A and 2B), and an increase in slip is observed to the SE of the epicenter bounded by two Tzz highs (zoom highlighted in Fig. 2B). In the SE ending of the rupture area, a slight increase in slip coincides with other Tzz relative minima (red circle in Fig. 2B). When exploring in-depth, by truncating Tzz up to N=200 (approx. 31km depth), a low Tzz anomaly is depicted (Fig. 2C) connecting the hypocenter location (33km) to the maximum slip patch 130 km to the southeast. This relative low Tzz to the SSE of the epicenter is probably indicating a heterogeneity that acted as a path to rupture propagation to the south (directivity) and further amplification (max. Slip patch) close to the Tzz minima lobe (<-2.5 Eötvös).

3.1.1.3. Seismic barrier at the Ilo peninsula

Many authors (e.g. Tavera et al., 2006; Audin et al., 2008) coincide that southward rupture propagation and migration of the aftershock sequence stopped near the Ilo Peninsula (area coincident with the location of the main aftershock on 7 July 2001, Mw=7.5, see Fig. 2A) suggesting the presence of an important seismic barrier. Bilek and Ruff (2002) observed

that no obvious tectonic feature exists in the subducting plate that could correspond with the southern termination of the rupture for these earthquakes (Mw=8.4 and Mw=7.7). Nevertheless, a landslide scar (right corner of Fig. 2A) is visible in the bathymetry (Smith and Sandwell, 1997; Amante and Eakins, 2009) between the trench and the coastline (Fig. 2A) as highlighted by Audin et al. (2008). The last authors proposed that there may be an influence of the upper plate forearc structure, particularly the Chololo Fault System and a series of similar faults that trend perpendicular to the trench, on the subduction plane segmentation probably constituting a barrier. They interpreted this fault set as progressive step faults that may have been triggered by gravitational effects during major subduction earthquakes. Another plausible explanation given in this study is that these faults may be susceptible to permanent deformation preventing the accumulation of the elastic strain energy necessary to sustain seismic rupture. Thus constitute a seismic barrier since historical earthquake ruptures are confined to the north and south of the Ilo peninsula (Dorbath et al., 1990; Audin et al., 2008).

Relative maximum in Tzz signal is mainly related to different types of subducting oceanic plate roughnesses (seamounts, aseismic ridges, etc.) controlling in a high degree seismic segmentation along the margin. At both lateral endings of the slip distribution, a narrowing of the gradient signal is observed, being the southern relative higher Tzz coincident with the bathymetric landslide scar highlighted by Audin et al. (2008) to the south of the Ilo peninsula (Fig. 2A). Inland, over the continental forearc, the Chololo Fault System (red circle of Fig. 2B) is depicted by Tzz (7.5 Eötvös) contours presenting a trend perpendicular to the trench.

Figure 3

3.1.1.4. Gravity disturbance and inversion model

The topography and sediment corrected gravity disturbance (Fig. 2D) from GOCE satellite-only model GO_CONS_GCF_2_DIR_R5 (Bruinsma, 2013) up to N=300 presents a relative minima (+25 mGal) close to maximum slip area, although with less resolution than Tzz. The trench parallel profile, along the marine forearc over maximum slip patch, shows that maximum slip is centered over gravity minima.

The inversion model depicts a low-density contrast in the region of maximum slip and high-density contrast along lateral rupture borders. The local gravity disturbance minimum (+30 mGal) that correlates to maximum slip (Fig. 11A) is related to lower densities in the inversion model, that could reflect a forearc basin over the continental shelf, developed as a consequence of the Nazca Fz subduction (Wells et al., 2003, Basset and Wats, 2015a). Muller and Landgrebe (2012) found that the occurrence of great megathrust earthquakes (M≥ 8) is strongly biased towards regions were oceanic fractures subduct. The last authors explained that Fz's generally have very large physical offsets and could play an important influence in interplate coupling. In this sense and particularly for this event the Nazca Fz increased the plate coupling between the two sides of the fault, resulting in a heterogeneous rupture, with the main stress release focussed on the Nazca Fz subduction zone intersection.

3.2. The Maule Mw=8.8 2010 earthquake

The Maule Mw=8.8 2010 earthquake initiated at approximately 36.5ºS (22.9 km ± 9.2 depth), and ruptured the subduction plate interface bilaterally through two major slip patches affecting approximately 500 km of the Nazca-South American interface (Delouis et al., 2010; Lay et al., 2010; Lorito et al., 2011; Moreno et al., 2012; Pollitz et al., 2011; Tong et al., 2010; Vigny et al., 2011). Even though these studies vary significantly in determined slip magnitude and location, they roughly coincide in the location of the northern patch between ~34.5ºS and 35.5ºS which concentrated the major slip (15 to 20 m). The 2010 Maule aftershocks and the coseismic slip ended to the south at the entering Mocha Fz, where the major asperity of the 1960 earthquake sequence is thought to have occurred (Lange et al., 2012; Lorito et al., 2011), existing a certain overlap between both ruptures. Moreno et al (2012) calculated the slip along the megathrust from a joint inversion of GPS, InSAR, and land-level changes data using Green's functions generated by a spherical finite-element model, being one of the best constrained models for this event.

3.2.1. Results:

3.2.1.1. Earthquake rupture behavior from Tzz

In a previous work, Alvarez et al. (2014) performed forward modeling with a former satellite GOCE model (GO_CONS_GCF_2_TIM_R4, Pail et al., 2011) developed up

degree/order N=250 finding an inverse relationship between both quantities. In that work, the northern maximum slip patch matches the minimum Tzz lobe. Then Alvarez et al. (2015a) explained that coseismic and postseismic slips (elastic rebound) after the Maule earthquake left a significant imprint over the gravimetric signal, detected as an increase of the signal along the coast-line by subsequent GOCE models when compared up to the same degree/order (N=250). This change in the gravity gradient signal worsens the relationship between both quantities when using the last model up to its maximum degree.

The topography and sediment corrected vertical gravity gradient calculated in this work up to N=300 (Fig. 4A) in the region of the Maule earthquake presents a first-order anti-correlation with the rupture model of Moreno et al (2012) along the outer marine forearc. However, the GOCE model used presents relative minima Tzz lobes shifted to the trench with respect to maximum slip patches (as expected according to the above-explained). An along-strike segmentation of Tzz is observed, over both the marine and continental forearc, coinciding the northern and southern slip patches with relative minima Tzz over the coastline and the continental forearc. A higher-order model incorporates on its frequency spectral content information of shallower structures, being necessary to develop the model at lower degree/orders (cutting) to unravel deeper anomalies that may be related to seismogenesis.

Figure 4

3.2.1.2. High Vp down dip seismic barriers and Tzz

Based on a seismic tomography Hicks et al. (2014) found a moderate Vp (5.5–7.0km/s, reduced Vp/Vs ratio of ~1.71 and a Poisson's ratio of 0.24), consistent with a granitic composition (Christensen, 1996) along the upper continental forearc (cf) beneath the Coastal Cordillera. In the lower forearc, they identified two prominent high Vp anomalies named Cobquecura and Pichilemu (with Vp 7.6–8.0km/s, Vp/Vs ratio of ~1.81 and Poisson's ratio of 0.28) lying beneath the coast (Vp model at 25km depth), coincident with a high positive Bouguer gravity anomaly (see fig. 8 from Hicks et al., 2014) for more detail). These authors suggested a moderate positive correlation between gravity and Vp in the lower forearc (Hicks et al., 2014).

The inspection of the Tzz map strengthens the proposal of Hicks et al. (2014) developed up to N=250/Z=25 km (Fig. 4B) where two highly positive Tzz regions roughly coincide in geometry with high Vp anomalies. These authors interpreted the seismic velocities and gravity signal associated with these anomalies as dense, ultramafic material, where coseismic slip was reduced, existing a general strong negative correlation between Vp and coseismic slip for the down-dip portion of the rupture. Moderate Vp found along the upper continental forearc (cf) coincides with relative minima in the gradient signal. Along strike segmentation of the gradient signal calculated in the present work at depths of 25 km (N=250) over the continental forearc, coincides with the Lanalhue (LF) and Pichilemu (PF) major upper plate faults (Moreno et al., 2012).

Kiser and Ishii (2011) interpreted that, for the high-frequency part of the rupture, there is a striking interaction with the velocity structure along the plate interface. Comparing forearc tomographic results with coseismic slip distribution from Moreno et al. (2012), Hicks et al. (2014) proposed that the rupture was slowed by the high-velocity anomalies beneath the coast, generating stopping phases at the rupture's down-dip termination (stepping down high-frequency energy released around the anomalies) and in part controlling the down-dip and along-strike distribution of slip during the rupture. The down-dip extension of the rupture region (defined by the 1-m slip contour from Moreno et al., 2012) reached depths of 55 km and 50 km in the north-central and south-central parts of the rupture zone, respectively. This down-dip limit for the rupture could be mapped also by a long-wavelength positive Tzz signal (Fig. 5), indicative of dense materials, mapped following the continental forearc for degree/orders 150<N<200 (between approximately 41km and 31km depth).

3.2.1.3. Asperities identification from Tzz

Previous works showed that for the Maule earthquake, the greatest coseismic slip and aftershock activity occurred at depths of the plate interface beneath the outer wedge (17–30km, "Domain B") where the plate interface is structurally more homogeneous (e.g. Hicks et al., 2014). The last authors found low Vp (4.75–6.25km/s) and a high Vp/Vs ratio (1.9–2.2, Poisson's ratio of 0.31–0.37) along the marine forearc, and moderate Vp (~6.5km/s) and elevated Vp/Vs ratio (~1.86) beneath the outer wedge. They interpreted these Vp

velocities as consistent with sediments and meta-sediments in the frontal prism and outer wedge. This is consistent with low Tzz lobes indicative of lower density materials along the marine forearc, as shown by Alvarez et al. (2014).

The slip model from Moreno et al. (2012) exhibits a concentration of high slip (up to 16 m) in the north-central part, and two secondary asperities with slip over 12 m at 36.1°S and 37°S respectively. The last authors found slips longer than 5 m in the Arauco Peninsula that propagated up to 50 km inland of the coastline while at the northern patch, large slips concentrated beneath the continental shelf. When truncating the GOCE model up to N=200 (Fig. 4C) reaching an auscultation depth of approximately 31km, the Tzz lobes (-10 Eötvös) match the maximum slip patches (It is important to highlight that the southern patch that was not resolved by Tzz in Alvarez et al., 2014). The along-strike extent of the rupture coincides both north and south with a narrowing of the signal (relatively higher Tzz), which would be indicating the location of attenuators/barriers to seismic energy release (as previously mentioned in Alvarez et al., 2014). The southern end of the rupture zone overlaps an area with low locking degree (Moreno et al., 2010), which may have arrested further southward propagation of the rupture (Moreno et al., 2012).

The last authors found a first-order spatial correlation of the interseismic locking patches with high coseismic slip regions for the Maule event. Similar results for the 2011 Tohoku-Oki earthquake were exposed by Loveless and Meade, (2011) and by Ozawa et al. (2011). As previously explained, Metois et al. (2016) found a first-order correlation between coseismic asperities and highly coupled segments for the three most recent Mw>8 events along the Chilean margin. The last authors also explained that most low coupling zones, which behaved as barriers effectively arresting ruptures propagation, correlate with subducted high oceanic features associated with crustal fault networks. Moreno et al. (2012) suggest that splay faults in the upper plate limited rupture propagation in the up-dip and along-strike directions. Major upper plate faults mapped by the last authors as the thrust ridge, the Santa María Fault and the Lanalhue Fault (Fig. 4C), agree with the Tzz signal up to N=200/Z=30 km. The TR is coincident with the up-dip limit to rupture propagation and is depicted by a high gradient signal of -5 Eötvös. A gradient signal narrowing observed at different degrees of the harmonic expansion (Fig. 4C) depicts the

Lanalhue Fault that cuts across the entire forearc affecting the morphology and displacing geological units.

Figure 5

3.2.1.4. Gravity disturbance and inversion model

Gravity disturbance relative minima (< +25 mGal) are close to high slip patches such as the previous relationship found with Tzz. Gravity minimum that matches the northern slip patch could be dominated by low-density materials filling a shelf basin (yellow dashed ellipse of Fig. 4D) centered at 35ºS. From a 2-D gravity modelling and the analysis of bathymetric profiles, Maksymowiccz et al. (2015) explained that main slip patches developed in a segment of the margin characterized (among other characteristics) by low-density materials in the continental wedge and a well-developed shelf basin, such as was also observed by Wells et al. (2003) for other circum-Pacific earthquakes. Previous works mapped asymmetric half-graben basins beneath the continental slope and well-developed shelf basins in this region; whereas the geometry of the slope basins is controlled by the displacements on the bordering faults that accommodate differential tectonic subsidence and/or uplift in the continental wedge (Díaz-Naveas, 1999; Contardo et al., 2008; Contreras-Reyes et al., 2010, 2013; Maksymowiccz et al., 2015). Moreno et al. (2012) proposed that slab inflections may also have influenced the apparent overshoot in the northern asperity (between 34°S - 36°S) and suggested that the plate geometry may influence strain accumulation and release in a subduction zone.

The harmonic decomposition of the Tzz shows a negative lobe which continues in depth up to higher orders (Fig. 5) and the local gravity disturbance minima (+15 mGal) centered at 35ºS that correlates to maximum slip (Fig. 4D) are related to lower densities in the inversion model. The gravity minima centred over the basin could also be indicating the effect of the subducted plane inflection noted in Moreno et al. (2012). Gravity field derivatives could indirectly map changes in the dip angle: Alvarez et al. (2015b) mapped anomalous Moho depth thickening at the sites of inception of four high oceanic features (between 24ºS and 34ºS), and residual free-air gravity anomaly from Basset and Watts (2015b) clearly maps regions of flat slabs subduction (Chilean-Pampean and Peruvian flat slabs).

The trench parallel profile, along the continental shelf cuts across maximum slip patches showing maximum slip centered over gravity relative minima. Alvarez et al. (2014) obtained similar results for Tzz from GOCE DIR-R4 model. In the present work, the distribution and geometry of mass heterogeneities obtained from the inversion model depict a low-density contrast in the regions of maximum slip and high-density contrasts along lateral rupture borders. Inversion models for Arequipa (Fig. 11A) and for Maule (Fig. 11B) present a very low-density contrast in-depth in regions where the Nazca plate presents important inflections as the subduction of the Nazca Fz and the along-strike inflection between 34°S - 36°S reported by Moreno et al. (2012). Maximum slip propagated towards these areas corresponds to basins developed over the continental shelf indicating a complex relationship between subducting slab morphology, upper plate deformation with basin development and rupture propagation behavior.

3.3. The Illapel Mw=8.3 2015 earthquake

On September 16 2015 a Mw=8.3 earthquake occurred offshore Chile, with epicentre location near Illapel at an estimated depth of 25.0 km (USGS - 31.570ºS, 71.654ºW) or 17.8 km (GCMT - 31.22°S, 72.27°W). The earthquake nucleated near the coast but then propagated northwards and up-dip, rupturing across the width of the seismogenic zone, with a maximum slip of 5-6 m, based on results obtained from a joint inversion of geodetic and seismological data sets (Tilmann et al., 2016). Several works (Lay et al., 2014; Tilmann et al., 2016; Shrivastava et al., 2016; Melgar et al., 2016) have agreed that high-frequency seismic radiation (HFSR) was mostly released downdip of the primary seismogenic zone (domain B), reaching both the shallow and tsunamigenic portion of the megathrust (domain A) and the deeper HFSR part (domain C) related to strong ground shaking. Along-strike rupture extension coincides approximately with a more highly coupled region of the megathrust (Tilmann et al., 2016; Métois et al., 2012). Fault geometry and location are consistent with the slip of the Nazca plate beneath the South American plate, as indicated by seismic source parameters. The Mw=8.3 Illapel earthquake occurred in a region with intermediate to low trench sediment infill, < 500m (Ranero et al., 2006; Völker et al., 2006). This region between the Juan Fernández aseismic ridge (JFR) and the Challenger Fracture Zone (Fz) was identified as a seismic gap based on the occurrence of previous

great earthquakes that affected the interplate zone (Abe, 1981; Beck et al., 1998 Kelleher, 1972; Nishenko, 1985).

3.3.1. Results:

3.3.1.1. The role of high oceanic features and their gravimetric expression

Rupture propagation roughly arrested at regions with lower interseismic coupling (Metois et al., 2016; Tilman et al., 2016) which coincide with subducted oceanic plate features: the JFR to the south and the Challenger Fz to the north respectively probably acting as seismic barriers (Alvarez et al., 2017a; Shrivastava et al., 2016). However, Tilman et al. (2016) proposed that these features limited the aftershock zone rather than rupture, the latter occupying a smaller area. In fact, aftershocks clustered around the area of maximum coseismic slip, and in particular in lateral and down-dip directions (Lange et al., 2016) and into areas of intermediate locking to the south and north (Tilmann et al., 2016, Metois et al., 2012).

Aftershocks clustered around individual subducted seamounts that are thought to cause pervasive fracturing around the plate boundary fault zone, in this event were related to the down thrusting JFR at the southern rupture boundary (Lange et al., 2016). Subduction of the JFR and high relief horst-and graben structures erode frontally and basally the margin resulting in the collapse of the seaward part of the overriding plate (Contreras-Reyes et al., 2015). Unfavorable conditions for rupture propagation of large subducted relief (>1000 m) (Sparkes et al., 2010) suggest that the subduction of the JFR controlled the southern boundary of the 2015 Illapel earthquake and the clustering of aftershocks between 32–33°S (Lange et al., 2016). The extrapolated Juan Fernández ridge beneath the South American Plate shows a segmentation of the +5 Eötvös contour (Fig. 6A), presenting a westward concave maximum relative in Tzz and in Ga (see Fig. 6B) related to the deformation produced by the JFR.

The extrapolation of the Challenger Fz under the marine forearc coincides with a relative maximum and a higher degree of narrowing of the Tzz signal than the expression of the JFR to the south, cutting off the -2.5 Eötvös contour. This region of relatively low interseismic coupling (Métois et al., 2012; Tilmann et al., 2016) could be favoured by plate interface creeping acting as a seismic barrier, since all great historical earthquakes stopped

at this feature (Sparkes et al., 2010; Contreras-Reyes and Carrizo, 2011, Shrivastava et al., 2016). The last author's proposed that the CFZ could be considered as a persistent and strong barrier and that the JFR acted as a weak barrier working efficiently during the 2015 event (see Shrivastava et al., 2016 for more details). This agrees with the proposal of Alvarez et al. (2014), who proposed that different degrees of attenuators/barriers to the propagation of seismic rupture could be mapped using along-strike segmentation of different relative maxima in Tzz.

3.3.1.2. Asperities identification from Tzz

The structure of Chilean margin to the north of the JFR subduction point is mainly erosive, with little sediments along the trench axis, and characterized by the presence of a subsided/collapsed outermost forearc material composed of highly fractured volcanic rocks (Contreras-Reyes et al., 2015). In this region, the Tzz over the marine forearc increases trench wards progressively and the Tzz minima lobe in this region (-2.5 Eötvös) is half wide than to the south of the JFR. This highly positive Tzz signal, at a high wavelength ~100km and a minimum auscultation depth of 21 km, masks small asperities in the up-dip portion of the interface (Domain A). In this domain most of the coseismic slip concentrated around a shallow (<20 km depth) seismic asperity (~100 km wide along-strike) according to Shrivastava et al. (2016), based on a GPS only model.

However, slip also propagated in the down-dip direction (between 20 and 40 km depth) to the east of the central part of the rupture with a substantial coseismic slip of 3-5 m (Tilman et al., 2016; Shrivastava et al., 2016; Melgar et al., 2016; Lange et al., 2016). Inland, slip contours concentrate over a relative minimum of Tzz (Fig. 6A), being the rupture flanked to north and south by higher Tzz values (more than +15 Eötvos). Highly positive Tzz in the down-dip portion of the megathrust could indicate the existence of seismic barriers at depth, both along and across strike (as previously observed for the Arequipa and Maule earthquakes).

Figure 6

Tzz minima lobe over the marine forearc continues in depth from harmonic decomposition (Fig. 7) up to approximately 30 km coinciding with NW rupture propagation direction. At

depths of 36 to 40 km, the effect of the subducting slab inhomogeneities (CFZ and JFR) dominates the gravity signal over the marine forearc. From these results, we can hypothesize that oceanic features highly influence rupture behavior in this region of the megathurst as proposed by previous authors (e.g. Sparkes et al., 2010; Contreras-Reyes and Carrizo, 2011, Shrivastava et al., 2016).

Figure 7

Inland, at these depths (150<N<175), next to the coastline, low Tzz values coincide with maxima slip and strong ground shaking, being these anomalies probably related to unstable areas of domain C (Lay et al., 2012). This lower gravity derived signal, flanked latitudinally by two separate maximums observed in the continental forearc using harmonic decomposition, is also depicted by the ***Gd*** (next section). This observation (and after the analysis of other events in previous works) reveals that in this region of the forearc the gravity field is also useful to determine heterogeneities with different behavior during rupture in the downdip portion of the megathrust, where the forearc structure seems to have a greater influence on the seismogenic behavior (Tassara, 2010).

3.3.1.3. Gravity disturbance and inversion model

The gravity disturbance (Fig. 6B) presents a smooth decrease throughout the marine forearc probably dominated by the effect of the subducting slab. Inflections of the contours of +50 mGal and +25 mGal coincide with the extrapolation of the subdtucted CFZ and JFR respectively. A minimum relative ***Gd*** lobe is depicted eastward to the coastline in the region where slip contours enter inland. Most slip and strong ground shaking in this region are supposed to come from down-dip conditionally stable areas of domain C (Lay et al., 2012). This lower ***Gd*** lobe (<25 mGal) characterizes an anomalous zone with higher slip, with better detail than the Tzz signal (Fig. 6A) which only shows a relative minimum in this region (close to the down-dip limit of the seismogenic zone). Previous findings indicated that the gravity disturbance is better than the Tzz for unveiling deeper source anomalies (Braitenberg et al., 2011; Alvarez et al., 2012). The inversion model depicts a high-density contrast both sides of the rupture and a deep and smooth concavity at the

center of the rupture even though Gd signal varies very little along the profile over the marine forearc.

3.4. The Pisagua 2014 M_w=8.2 earthquake

On April 1, 2014 a M_w=8.2 earthquake initiated at ~ 95 km NW of Iquique, at a depth of about 20 km, with both epicentre and focal mechanism consistent with an event that ruptured the plate boundary interface between the Nazca and South America plates (Ruiz et al., 2014; Bürgmann, 2014; Schurr et al., 2014; Moreno et al., 2014; Lay et al., 2014). To the south, the largest historical earthquake occurred in 1877 (Iquique event) with magnitude Mw ~ 8.5-8.8 (Lomnitz, 2004), and estimated rupture zone from Arica to Antofagasta. This zone was recognized as the Iquique seismic gap in northern Chile, with a return period varying from ~ 111 to 264 yr (Nishenko, 1985; Comte and Pardo, 1991; Chlieh et al., 2011). The Iquique rupture affected an area of intermediate to high interseismic coupling (Metois et al., 2013; Schurr et al., 2014; Ruiz et al., 2014) and rupture propagation accelerated downdip following the gradient towards higher locking with a peak slip of 8 m to the southeast of the hypocentre at depths of 30-40 km (Schurr et al., 2014; Hayes et al., 2014). Slip models coincide in showing a very compact rupture area for an earthquake of this size, and rupture did not penetrate the low coupling zones (Hayes et al., 2014; Ruiz et al., 2014). Slip models also agree that earthquake rupture diminished towards the shallow-most up-dip part of the subduction zone (Geersen et al., 2015).

3.4.1. Results:

3.4.1.1. The relation between subducted seafloor roughness and foreshock activity to the gravimetric signal of Tzz

An intense foreshock activity developed in the previous months to the main event (with seismic swarms since 2005), which accelerated towards the final foreshock sequence, with a slow slip event on the interplate preceding the 2014 Iquique earthquake (Ruiz et al., 2014). Schhur et al. (2014) inferred gradual unlocking of the plate interface and physical changes at the plate boundary from a decrease in b value three years before earthquake occurrence. These smaller asperities ruptured progressively by foreshocks will have loaded the remaining larger asperities in this zone until their failure (Schhur et al., 2014). Geersen

et al. (2015) imaged multiple large seamounts along the plate interface under the marine forearc in the intermediate coupled central part (19º to 20.5º S) of the northern Chile seismic gap, from marine seismic reflection and swath bathymetric data. These authors proposed that those subducting seamounts likely exert primary control on regional-scale plate-coupling variations and that limited the up-dip and southward extent of the seismic rupture during the 2014 earthquake.

The area that ruptured during the 2014 Iquique earthquake matches the width of the subducted Iquique Ridge (Fig. 8) under the marine forearc (Metois et al. 2013; Rosenbaum et al. 2005; Geersen et al. 2015). At degrees higher than N=200, relative lower Tzz values (<+10 Eötvös) over the Nazca Plate indicate crustal flexure from loading associated with seamounts related to the IR, indicating a segmentation of the forebulge (Fig. 8A, B, C).

Figure 8

Schurr et al. (2014) proposed that the Iquique segment seems to have been dominated by mostly smaller locked asperities embedded in a conditionally stable environment, this precludes identifying an inverse relationship between Tzz and slip patches due to the high wavelength characteristic of GOCE signal. In fact, slip patch for this earthquake shows no clear correlation to a minimum Tzz lobe, although a narrowing of the signal to the north and south coincides with rupture ending (Fig. 8B). For this region, the density structure morphology presents a distinct behavior as auscultation depth increases, in contrast to what was analyzed for the other events (where minima Tzz lobes match to maximum slip). As auscultation depth increases (N≤200), is observed a positive Tzz signal for over the maximum slip region.

Another hypothesis suggests that subducted lower reliefs may act not only as barriers but also as asperities linked to seismic rupture (Husen et al., 2002; von Huene et al., 2012; Bilek et al., 2003) depending on earthquake rupture nucleation location. Many studies indicate that subducting seamounts generate networks of small-scale fractures and faults causing unfavorable conditions for seismic rupture propagation, as observed in high-resolution seafloor images and reproduced in analog modeling (Cloos, 1992; Mochizuki et al., 2008; Dominguez et al., 2000; Wang and Bilek, 2011; Kopp, 2013). Some works (Sobiesiak et al., 2007; Llenos and McGuire, 2007; Tassara, 2010) already focused on these

Central Andean forearc asperities and their link to gravity highs (mafic bodies) reflected in a high-VSA. In the Southern Andes, the forearc is felsic-dominated (low-density) producing neutral-to-negative VSA (being VSA the Vertical Stress Anomaly that accounts for the component of normal stress due to the weight of the overlying crustal column; Tassara 2010). In this sense, a high Tzz signal is observed over maximum slips for N= 200 (Z=31km) in a region dominated by a lack of sediments along the trench and basal tectonic erosion of the forearc crust. For N=150 (Fig. 8D) an eastward inflection of the +10 Eötvös contour is observed in the area where the foreshock sequence and maximum slips took place. This highly positive signal could be related to subducted seamounts and basal erosion associated with the subduction of the Iquique ridge (Alvarez et al., 2018a).

Down-dip rupture propagation ending correlates with a high Tzz signal across the continental forearc beneath the coastline, as observed for the other earthquakes analyzed. The main aftershock on April 3, 2014 an M_w=7.7 propagated further inland over a region with relative lower Tzz signal, as exposed by Alvarez et al. (2015a).

Figure 9

3.4.1.2 Gravity disturbance and inversion model

The gravity disturbance presents a wide inflection of the +75 mGal contour coinciding with the extrapolation of the subducted Iquique ridge. This change in the gravity signal is more abrupt to the north where a subducted seamount is clearly depicted by the bathymetry (ETOPO1). Rupture coincides with this relative higher gravity as shown by Tzz at degrees between 150<N<200. Such a correlation is expected as gravity anomaly depicts deeper mass sources than Tzz when compared at the same degree/order. The fact that rupture coincides with a relatively higher gravity signal (and deeper Tzz anomalies) reinforces the hypothesis that the IR exerted a primary control on this earthquake nucleation and rupture propagation rather than shallower marine forearc structures. The inversion model (Fig. 20) depicts a high-density contrast both sides of the rupture and a deep and smooth concavity close to the epicenter.

Figure 10

Figure 11

4. Discussion

4.1. Events Nucleation

After the analysis of the GOCE signal up to the maximum degree of the harmonic expansion N=300 (maximum spatial resolution and shallower sources), we observed that the Mw>8.0 earthquakes nucleated close to a local positive high gradient zone to the coastline. In this sense, Tassara (2010) previously showed that ruptures along the Andean margin generally nucleated at the edge of geological heterogeneities in the forearc. Hicks et al. (2014) reported that the Maule earthquake nucleated in a region of high Vp (~7.2km/s) and strong dip-parallel Vp gradient, at the periphery of the Cobquecura anomaly. They suggested a positive correlation between Vp and a high positive Bouguer gravity anomaly, explaining that a local increase in stress at the edge of this anomaly could have led to the onset of the rupture. The higher spatial resolution that can be obtained from satellite GOCE allows mapping different anomalies along the forearc with better detail than ever before. Additionally, the Tzz allows mapping shallower geological structures and mass heterogeneities with greater detail than the gravity anomaly (Bouguer), as performed by other authors formerly. This improvement could help to infer probable future earthquake nucleation areas using Tzz maps along different coasts of the Earth.

4.2. Downdip rupture limit

Wells et al. (2003) exposed that seismic slip decreases landward across a strong gravity gradient marking the landward edge of the forearc basins and deep-sea terrace in most cases. Kopp (2013) explained that the limited downdip extent of the seismogenic zone is also supported by gravity data and thermal modeling (Grevemeyer and Tiwari, 2006) as well as by the forearc morphology (Krabbenhoeft et al., 2010). From the analysis of ruptures of historical great megathrust earthquakes along the Chilean margin, Alvarez et al. (2014) noticed that many ruptures arrested to the west of a positive Tzz anomaly (more than +10 Eötvös), and proposed that this high could potentially reveal the location of a seismic barrier marking the eastern edge of rupture propagation. Basset and Watts (2015) already correlated the high gravity signal along the coast to the downdip limit of the seismogenic region with high coseismic slip and strong plate coupling and that minimal coseismic slip occurred landwards of this gravity high. In this work, using detailed analyses

of higher resolution Tzz (at different degrees of the harmonic expansion), we infer that this highly positive signal, when calculated at N=200 and the corresponding depth of approx. 30 km, could be indicating the down-dip limit of the seismogenic zone. On the other hand, relative minima under in this coastal region (continental forearc), where slip increased, could be unveiling smaller asperities typical of domain C.

4.3. Directivity effect

Different approaches have been tested to explain earthquake directivity. McGuire et al. (2002) found, in a global analysis, that most earthquakes are unilateral, and fault segmentation might explain this observation for large earthquakes. Other authors (Rubin and Gillard, 2000; Pritchard et al., 2007) proposed as alternative explanations the history of previous earthquake ruptures, preferential orientation of structures on the fault interface due to oblique convergence or the superposition of different materials across the fault zone.

For the 2001 Arequipa earthquake, the gravity signal shows a "path" of relative low Tzz that matches unilateral rupture propagation towards the southeast, as mapped from seismological studies (Giovanni et al., 2002; Pritchard et al., 2007; Robinson et al., 2006; Salichon et al., 2003; Swenson and Beck, 1999). Positive Tzz (+5 Eötvös contour) to the SE, NW and W of the hypocenter could be indicating different material properties impeding rupture propagation in those directions.

4.4. Asperities and Along Strike Seismic Segmentation

Relative maxima in Tzz along strike are well correlated to slip decrease and also to lateral rupture ending, as exposed by Alvarez et al. (2014), implying that high Tzz could be related either to the forearc structure as splay faults or to subducted high oceanic features acting as seismic barriers. Minima Tzz lobes are highly related to slip increase (Alvarez et al., 2014, 2015a) and to regions where the rupture propagates, except for Iquique earthquake where the rupture seems to have nucleated over subducted plate roughnesses.

Different trench parallel profiles along the marine forearc over maximum slip patches for the analyzed events, shows that maximum slip is centered over gravity disturbance minima, but with higher resolution than previous works (Song and Simons, 2003; Wells et al., 2003).

The analysis at different depths (by cutting de degree/order) shows a better correlation between slip and Tzzz signal when using N=200 (z=30km). At this minimum depth, Tzz lobes could be indicating regions with a homogeneous asperity distribution related to a smooth and strongly coupled interface, typical of domain B (Fig. 12). This domain is characterized by large and relatively uniform regions with unstable sliding frictional properties (asperities) and large slip (at source depths spanning from 15 to 30 km) where most megathrust events occur Lay et al. (2012).

4.5 Seismic segmentation along the continental forearc

The high gravity gradient to the coastal line that marks the downdip limit of the seismogenic zone presents an along-strike segmentation where relative low interposed Tzz values coincide with slip increase over the continental forearc. Particularly for the Maule earthquake, these relative minima in the gradient signal are close to regions of lower Vp. Thus by using Tzz and Gd, it would be possible to map smaller heterogeneities over the continental forearc. This higher achieved resolution is of great importance since the ruptures analyzed (e.g. the southern patch of the Maule earthquake, the Iquique main aftershock, the Illapel rupture and the small increase in slip for Arequipa earthquake), occurred inland over the downdip limit of the seismogenic zone and correlate to relative minimum in Tzz signal over the continental forearc (see Fig. 12). Whether these relative minima of the signal inland are shallower effects (ground effects) mainly at high orders (less depth) or deeper asperities typical of the domain, C (observed at lower orders) is a matter of future works. Along and across strike segmentation of the coastal Tzz highs and interspersed gravity lows greatly improve the mapping of heterogeneities located over the downdip limit with respect to previous works, and could serve as a proxy of seismogenic behavior of densely populated coastal areas.

4.6 The "distinct" behavior of the 2014 Pisagua-Iquique (Chile) earthquake sequence

A comparison between the 2010 Maule and 2014 Iquique sequences highlights the broad range of seismotectonic behavior that could be expected along the same subduction zone, leading up to and in response to megathrust ruptures (Hayes et al., 2014). Schurr et al. (2014) concluded that gradual weakening of the central part of the seismic gap accentuated

by the foreshock activity in a zone of intermediate seismic coupling was instrumental in causing final failure, distinguishing the Iquique earthquake from most great earthquakes. Lay (2015) also highlighted that the large slip for this earthquake was unusually concentrated for a great earthquake.

At the latitudes of the Pisagua earthquake, the Chilean margin has been characterized as erosive (von Huene and Scholl, 1991; Laursen et al., 2002; Adam and Reuther, 2000; Völker et al., 2006). In this region of the Andes, subduction erosion processes have been related to the morphological roughness of the oceanic plate and to the climate-related lack of sediments within the trench (Ranero et al., 2006) being the gradient signal along the marine forearc more positive than in the other analysed regions (were sediment accretion has been reported as to the south of JFR and with well developed shelf basins).

From this work, we can observe that the gravity signal presents a distinct behavior for the Pisagua earthquake when compared to the other events analyzed. Harmonic decomposition shows Tzz maxima in the region of maximum slip for degrees between 150<N<200 being a plausible explanation that this gravity high is related to the subducted IR, favoring the hypothesis that subducion of the IR played a key role in rupture propagation (the intense foreshock sequence has been associated with subducted seamonts). In recent work, Alvarez et al. (2018a), found differential variations of geoid heights along the marine forearc related to IR subduction. These results agree with along-strike variation in coupling from Metois et al. (2012) and Ruiz et al. (2014), with fore-slip models (Socquet et al., 2017), and to slip models (e.g. Schurr et al. 2014; Socquet et al. 2017). In this sense, it would be possible to associate negative Tzz to sediments accretion, positive Tzz to subduction erosion and consequently to distinct rupture behaviors depending on the tectonic setting.

5. Conclusions

Many authors coincide that interseismic strain is transformed into permanent forearc geologic strain via faulting, folding or buckling which leaves a deformation imprint that could remain relatively stable throughout the repetition of the seismic cycle along the Chilean margin. Gravity signal is in part the expression of dynamic processes along the margin such as uplift, long-term subsidence, erosion and accretion processes, reflecting plate interactions.

Along the Chilean margin, where data show a seismic segmentation, co-seismic slip distribution tends to concentrate along forearc basins (Wells et al., 2003, Song and Simons, 2003) and structural heterogeneities correlate with forearc features (Tassara, 2010) which probably modulated along strike by downgoing plate heterogeneities (Hicks et al., 2014, Basset and Watts, 2015). In this framework, GOCE gravity derived signal allowed mapping along and across strike heterogeneities related to seismic rupture behavior, geological structures and velocity anomalies.

Figure 12

From the analysis of the last Mw>8.0 earthquakes along the Peru-Chilean margin, we found that meghathrust slip behavior is highly related to density structure along the seismogenic zone as revealed by GOCE gradients. The relationship between high/low coupling with higher/lower slip patches observed by other authors is now mapped by relatively low/high Tzz; thus demonstrating the usefulness of the gravity derived signal as a first-order proxy for mapping asperities and barriers along the seismogenic zone (Fig. 12). The methodology used in the present work could help to better mapping physical properties along the plate interface to determine regions with higher seismic hazard; also by mapping forearc gravity high anomalies, related to mass heterogeneities, it is possible to infer probable nucleation areas. Tzz minima distribution along the marine forearc is well correlated to slip maxima and could serve to estimate seismic hazard close to densely populated coastal regions.

Acknowledgments: Authors acknowledge the use of the GMT-mapping software of Wessel and Smith (1998). The authors would like to thank to CONICET for founding. Satellite GOCE models and derived data (Tzz, Ga, Gd) can be downloaded from the International Centre for Global Earth Models (ICGEM) http://icgem.gfz-potsdam.de/home

References

Abe, K., 1981. Magnitudes of large shallow earthquakes from 1904 to 1980. Phys. Earth Planet. Int. 27, 72-92. https://doi.org/10.1016/0031-9201(81)90088-1

Adam, J., Reuther, C.D., 2000. Crustal dynamics and active fault mechan ics during subduction erosion. Application of frictional wedge analysis on to the North Chilean Forearc. Tectonophysics 321(3), 297–325. http://doi.org/10.1016/S0040-1951(00)00074-3

Alvarez, O., Gimenez, M.E., Braitenberg, C., Folguera A., 2012. GOCE satellite derived gravity and gravity gradient corrected for topographic effect in the South Central Andes region. Geophys. J. Int. 190 (2), 941-959. http://dx.doi:10.1111/j.1365-246X.2012.05556.x

Alvarez O., Gimenez, M.E., Braitenberg, C., 2013. Nueva metodología para el cálculo del efecto topográfico para la corrección de datos satelitales. Rev. Asoc. Geol. Arg. 70 (4), 422-429.

Alvarez, O., Nacif, S., Gimenez, M., Folguera, A., Braitenberg, A., 2014. GOCE derived vertical gravity gradient delineates great earthquake rupture zones along the Chilean margin. Tectonophysics 622, 198-215. http://dx.doi.org/10.1016/j.tecto.2014.03.011

Alvarez, O., Nacif, S., Spagnotto, S., Folguera, A., Gimenez, M.,Chlieh, M., Braitenberg, C. 2015a. Gradients from GOCE reveal gravity changes before Pisagua Mw=8.2 and Iquique Mw=7.7 large megathrust earthquakes. J. S. Am. Earth Sci. 64 (P2), 15-29. http://dx.doi.org/10.1016/j.jsames.2015.09.014

Alvarez, O., Gimenez, M., Folguera, A., Spagnotto, S., Bustos, E., Baez,W., Braitenberg, C., 2015b. New evidence about the subduction of the Copiapó ridge beneath South America, and its connection with the Chilean-Pampean flat slab, tracked by satellite GOCE and EGM2008 models. J. Geodyn. 91(C), 65-88. http://dx.doi.org/10.1016/j.jog.2015.08.002

Álvarez, O., Pesce, A., Gimenez, M., Folguera, A. Soler, S. Chen, W., 2017a Analysis of the Illapel Mw=8.3 thrust earthquake rupture zone using GOCE derived gradients. Pure App. Geophys. 174(1), 47-75. https://doi.org/10.1007/s00024-016-1376-y

Álvarez, O., Folguera, A., Gimenez, M.E., 2017b. Rupture area analysis of the Ecuador (Musine) Mw=7.8 thrust earthquake on april 16 2016, using GOCE derived gradients. Geod. Geodyn. 8, 49-58. http://dx.doi.org/10.1016/j.geog.2017.01.005

Álvarez, O., Gimenez, M., Guillen, S., Tocho, C., Folguera, A., 2018a. Goce derived geoid changes before the Pisagua 2014 earthquake. Geod. Geodyn. 9, 50-56. https://doi.org/10.1016/j.geog.2017.09.005

Álvarez, O., Gimenez, M.E., LinceKlinger, F., Folguera, A., Braitenberg, C., 2018b. The Peru-Chile margin from global gravity field derivatives. In: The evolution of the Chilean-Argentinean Andes, Chapter 3. Eds: Folguera, A., Contreras Reyes, E., Heredia, N., Encinas, A., Iannelli, S., Oliveros, V., Dávila, F., Collo, G., Giambiagi, L., Maksymowicz, A., Iglesia Llanos, P., Turienzo, M., Naipauer, M., Orts, D., M., Litvak, V., Alvarez, O., Arriagada, C. Springer Earth System Sciences. Springer, Cham. eBook ISBN: 978-3-319-67774-3, http://dx.10.1007/978-3-319-67774-3

Amante, C., Eakins, B.W., 2009. ETOPO1, 1 Arc-Minute Global Relief Model: Procedures, Data Sources and Analysis. NOAA Technical Memorandum NESDIS NGDC-24, 19 pp, March 2009.

Audin, L., Lacanb, P., Tavera, H., Bondoux, F., 2008. Upper plate deformation and seismic barrier in front of Nazca subduction zone: The Chololo fault system and active tectonics along the coastal cordillera, southern Peru. Tectonophysics 459 (1-4), 174-185. https://doi.org/10.1016/j.tecto.2007.11.070

Barazangi, M., Isacks, B.L., 1976. Spatial distribution of earthquakes and subduction of the Nazca plate beneath South America. Geology 4 (11), 686-692. https://doi.org/10.1130/0091-7613(1976)4<686:SDOEAS>2.0.CO;2

Barthelmes, F., 2013. Definition of functionals of the geopotential and their calculation from spherical harmonic models. Theory and formulas used by the calculation service of the International Centre for Global Earth Models (ICGEM). Scientific Technical Report, STR09/02, Revised edition, Jannuary2013. GFZ German Research Centre for Geosciences, Postdam, Germany. http://icgem.gfz-postdam.de/ICGEM

Bassett, D., Watts, A.B., 2015a. Gravity anomalies, crustal structure, and seismicity at subduction zones: 1. Seafloor roughness and subducting relief. Geochem. Geophys. Geosyst. 16, 1508-1540. https://doi.org/10.1002/2014GC005684

Bassett, D., Watts, A.B., 2015b. Gravity anomalies, crustal structure, and seismicity at subduction zones: 2. Interrelationships between fore-arc structure and seismogenic behavior. Geochem. Geophys. Geosyst. 16, 1541-1576. https://doi.org/10.1002/2014GC005685

Beck, S.L., Ruff, L.J., 1989. Great earthquakes and subduction along the Peru trench. Phys. Earth Planet. Int. 57, 199–224. https://doi.org/10.1016/0031-9201(89)90112-X

Beck, S., Barrientos, S., Kausel, E., Reyes, M., 1998. Source characteristics of historic earthquakes along the central Chile subduction zone. J. S. Am. Earth Sci. 11, 115-292, https://doi.org/10.1016/S0895-9811(98)00005-4

Bilek, S.L., Lay, T., 1999. Rigidity variations with depth along interplate megathrust faults in subduction zones. Nature 400, 443–446. https://doi.org/10.1038/22739

Bilek, S.L., Lay, T., 2002. Tsunami earthquakes possibly widespread manifestations of frictional conditional stability. Geophys. Res. Lett. 29 (14), 18-1,18-4. https://doi.org/10.1029/2002GL015215

Bilek, S.L., Ruff, L.J., 2002. Analysis of the 23 June 2001 Mw = 8.4 Peru underthrusting earthquake and its aftershocks Geophys. Res. Lett. 29 (20), 21-1, 21-4. https://doi.org/10.1029/2002GL015543

Bilek, S.L., Schwartz, S.Y., De Shon, H.R., 2003. Control of seafloor roughness on earthquake rupture behavior. Geology 31 (5), 455–458. https://doi.org/10.1130/0091-7613(2003)031<0455:COSROE>2.0.CO;2

Bilek, S.L., 2007. Influence of subducting topography on earthquake rupture. In: Dixon, T., Moore, J.C. (Eds.), The Seismogenic Zone of Subduction Thrust Faults. Columbia University Press.

Boulanger, O., Chouteau, M. 2001. Constraints in 3D gravity inversion. Geophys. Prosp. 49, 265-280. https://doi.org/10.1046/j.1365-2478.2001.00254

Bouman, J., Fuchs, M., Haberkorn, C., Lieb, V., Schmidt, M., Broerse, T., Schrama, E., Vermeersen, B., Visser, P., 2012. The Earth's time-variable gravity field observed by GOCE. GOCE Solid Earth Workshop, Enschede 16-17/10/2012

Bouman, J., Ebbing, J., Fuchs, M., 2013. Reference frame transformation of satellite gravity gradients and topographic mass reduction. J. Geophys. Res., Solid Earth, 118 (2), 759-774. https://doi.org/10.1029/2012JB009747

Braitenberg, C., 2014. Exploration of tectonic structures with GOCE in Africa and across-continents. Int. J. App. Earth Obs. Geoinf. 35 (A), 88-95. https://doi.org/10.1016/j.jag.2014.01.013

Braitenberg, C., Mariani, P., Ebbing, J., Sprlak, M., 2011. The enigmatic Chad lineament revisited with global gravity and gravity-gradient fields, in The Formation and Evolution of Africa: A Synopsis of 3.8 Ga of Earth History, Geol. Soc. London Spec. Publ. Vol. 357, pp.

329–341, eds Van Hinsbergen, D.J.J., Buiter, S.J.H., Torsvik, T.H., Gaina, C., Webb, S.J., Geological Society, London, https://doi.org/10.1144/SP357.18.

Bruinsma, S.L., Marty, J.C., Balmino. G., Biancale, R., Förste, C., Abrikosov, O., Neumayer, H., 2010. GOCE gravity field recovery by means of the direct numerical method. In: Lacoste-Francis H (ed) Proceedings of the ESA living planet symposium, Bergen, Norway, ESA Publication (27) SP-686

Bruinsma, S.L., Förste, C., Abrikosov, O., Marty, J.C., Rio, M.H., Mulet, S., Bonvalot, S. 2013. The new ESA satellite-only gravity field model via the direct approach. Geophys. Res. Lett. 40, 3607-3612. https://doi.org/10.1002/grl.50716

Bürgmann, R., 2014. Warnig signs of the Iquique earthquake. Nature 512, 258-259. https://doi.org/10.1038/nature13655

Chaves, C.A.M., Ussami, N., 2013. Modeling 3-D density distribution in the mantle from inversion of geoid anomalies: Application to the Yellowstone Province. J. Geophys. Res., Solid Earth, 118, 6328–6351, https://doi.org/10.1002/2013JB010168.

Chlieh, M., Perfettini, H., Tavera, H., Avouac, J., Remy, D., Nocquet, J., Rolandone, F., Bondoux, F., Gabalda, G. and Bonvalot, S., 2011. Interseismic coupling and seismic potential along the Central Andes subduction zone. J. Geophys. Res. 116, B12405, https://doi.org/10.1029/2010JB008166.

Christensen, N.I., 1996. Poisson's ratio and crustal seismology. J. Geophys. Res. 101, 3139–3156. http://dx.doi.org/10.1029/95JB03446.

Cloos, M., 1992. Thrust-type subduction zone earthquakes and seamount asperities: A physical model for seismic rupture. Geology 20 (7), 601-604. https://doi.org/10.1130/0091-7613(1992)020<0601:TTSZEA>2.3.CO;2

Comte, D., Pardo, M., 1991. Reappraisal of Great Historical Earthquakes in the Northern Chile and Southern Peru Seismic Gaps. Natural Hazards 4 (1), 23-44. https://doi.org/10.1007/BF00126557

Contardo, X., Cembrano, J., Jensen, A., Diaz-Naveas, J., 2008. Tectono-sedimentary evolution of marine slope basins in the Chilean forearc (33º30'–36º50'S): insights into their link with the subduction process. Tectonophysics 459, 206–218. https://doi.org/10.1016/j.tecto.2007.12.014

Contreras-Reyes, E., Flueh, E.R., Grevemeyer, I., 2010. Tectonic control on sediment accretion and subduction off south central Chile: implications for coseismic rupture processes of the 1960 and 2010 megathrust earthquakes. Tectonics 29, TC6018. http://dx.doi.org/10.1029/2010TC002734

Contreras-Reyes, E., Carrizo, D., 2011. Control of high oceanic features ans subduction channel on earthquake ruptures along the Chile-Peru subduction zone. Phys. Earth Planet. In. 186, 49-58. http://dx.doi.org/10.1016/j.pepi.2011.03.002

Contreras-Reyes, E., Jara, J., Maksymowicz, A., Weinrebe, W., 2013. Sediment loading at the southern Chilean trench and its tectonic implications. J. Geodyn. 66, 134–145. http://dx.doi.org/10.1016/j.jog.2013.02.009

Contreras-Reyes, E., Ruiz, J.A., Becerra, J., Kopp, H., Reichert, C., Maksymowicz, A., Arriagada, C., 2015. Structure and tectonics of the central Chilean margin (31°–33°S): implications for subduction erosion and shallow crustal seismicity. Geophys. J. Int. 203, 2, 776–791, https://doi.org/10.1093/gji/ggv309

Delouis, B., Nocquet, J., Vallée, M., 2010. Slip distribution of the February 27, 2010 Mw=8.8 Maule earthquake, central Chile, from static and high-rate GPS, InSAR, and broadband teleseismic data. Geophys. Res. Lett., 37. https://doi.org/10.1029/2010GL043899

De Mets, C., Gordon, R.G., Argus, D.F., 2010. Geologically current plate motions. Geophys. J. Int. 181, 1-80, http://dx.doi.org/10.1111/j.1365-246X.2009.04491.x.

Diaz-Naveas, J., 1999. Sediment subduction and accretion at the Chilean Convergent Margin between 35º and 40ºS. Dissertation zur Erlangung des Doktorgrades, Christian-Albrechts-Universitat zu Kiel (130 p).

Divins, D.L., 2003. Total Sediment Thickness of the World's Oceans and Marginal Seas, NOAA National Geophysical Data Center, Boulder, CO. https://www.ngdc.noaa.gov/mgg/sedthick/sedthick.html

Dominguez, S., Malavieille, J., Lallemand, S.E., 2000. Deformation of accretionary wedges in response to seamount subduction: Insights from sandbox experiments. Tectonics 19 (1), 182-196. https://doi.org/10.1029/1999TC900055.

Dorbath, L., Cisternas, A., Dorbath, C., 1990. Assessment of the size of large and great historical earthquakes in Peru. Bull. Seismol. Soc. Am. 80 (3), 551-576.

https://pubs.geoscienceworld.org/ssa/bssa/article-abstract/80/3/551/119293/assessment-of-the-size-of-large-and-great?redirectedFrom=fulltext

Ebbing, J., Braitenberg, C., Wienecke, S., 2007. Insights into the lithospheric structure and tectonic setting of the Barents Sea region from isostatic considerations. Geophys. J. Int. 171, 1390-1403. https://doi.org/10.1111/j.1365-246X.2007.03602.x

Featherstone, W., 1997. On the use of the geoid in geophysics: a case study over the north west shelf of Australia. Exploration Geophysics 28, 52–57. https://doi.org/10.1071/EG997052

Forsberg R., Tscherning C.C., 1997. Topographic effects in gravity field modelling for BVP. In: Sansó F., Rummel R. (eds) Geodetic Boundary Value Problems in View of the One Centimeter Geoid. Lecture Notes in Earth Sciences, vol 65. Springer, Berlin, Heidelberg. https://doi.org/10.1007/BFb0011707

Geersen, J., Ranero, C.R., Barckhausen, U., Reichert, C., 2015. Subducting seamounts control interplate coupling and seismic rupture in the 2014 Iquique earthquake area. Nature Com. 6, 8267. https://doi.org/10.1038/ncomms9267

Giovanni, M.K., Beck, S.L., Wagner, L., 2002. The June 23, 2001 Peru earthquake and the southern Peru subduction zone. Geophys. Res. Lett. 29 (21) https://doi.org/10.1029/2002GL015774.

Grevemeyer, I., Tiwari, V.M., 2006. Overriding plate controls spatial distribution of megathrust earthquakes in the Sunda–Andaman subduction zone. Earth Planet. Sci. Lett. 251, 199-208. https://doi.org/10.1016/j.epsl.2006.08.021

Grombein, T., Heck, B., Seitz, K., 2010. Untersuchungen zur effizienten Berechnung topographischer Effekte auf den Gradiententensor am Fallbeispiel der Satelliten gradiometrie mission GOCE. Karlsruhe Institute of Technology, KIT Scientific Reports 7547, pp. 1–94, ISBN 978-3-86644-510-9.

Grombein, T., Heck, B., Seitz, K., 2013.Optimized formulas for the gravitational field of a tesseroid. J. Geod. 87, 645-600. https://doi.org/10.1007/s00190-013-0636-1

Hayes, G.P., Herman, M.W., Barnhart, W.D., Furlong, K.P., Riquelme, S., Benz, H.M., Bergman, E., Barrientos, S., Earle, P.S., Samsonov, P., 2014. Continuing megathrust earthquake potential in Chile after the 2014 Iquique earthquake. Nature 512, 295-298. https://doi.org/10.1038/nature13677

Heck, B., Seitz, K., 2007. A comparison of the tesseroid, prism and point mass approaches for mass reductions in gravity field modeling. J. Geod. 81, 2, 121-136. https://doi.org/10.1007/s00190-006-0094-0.

Hicks, S.P., Rietbrock, A., Rydera, I.M.A., Lee, C.S., Miller, M., 2014. Anatomy of a megathrust: The 2010 M8.8 Maule, Chile earthquake rupture zone imaged using seismic tomography. Earth Planet. Sci. Lett. 405, 142-155. http://dx.doi.org/10.1016/j.epsl.2014.08.028.

Hofmann-Wellenhof, B., Moritz, H., 2006. Physical Geodesy, 2nd edn, pp. 286. Springer, Berlin. https://doi.org/10.1007/978-3-211-33545-1

Horton, B.K., 2018. Tectonic regimes of the central and southern Andes: Responses to variations in plate coupling during subduction. Tectonics 37, 402-429, https://doi.org/10.1002/2017TC004624

Husen, S., Kissling, E., Quintero, R., 2002. Tomographic evidence for a subducted seamount beneath the Gulf of Nicoya, Costa Rica: The cause of the 1990 Mw = 7.0 Gulf of Nicoya earthquake. Geophys. Res. Lett. 29 (8), 1238. https://doi.org/10.1029/2001GL014045.

Janak, J., Sprlak, M., 2006. New Software for Gravity Field Modelling Using Spherical Armonic. Geod. Cartog. Hor. (Geodetický a kartografický obzo), 52, 1-8 (in Slovak).

Jordan, T.E., Isacks, B.L., Allmendinger, R.W., Brewer, J.A., Ramos, V.A., Ando, C.J., 1983. Andean tectonics related to geometry of subducted Nazca plate. Geol. Soc. Ame. Bull. 94 (3), 341-361. https://doi.org/10.1130/0016-7606(1983)94<341:ATRTGO>2.0.CO;2

Kelleher, J.A., 1972. Rupture zones of large South American earthquakes and some predictions. J. Geophys. Res. 77, 2087-2103. https://doi.org/10.1029/JB077i011p02087

Kikuchi, M., Yamanaka, Y., 2001. Earthquake Information Center EIC Seismological Note Nº 105, Earthquake Res. Inst., Univ. of Tokyo, Tokyo. http://wwweic.eri.u-tokyo.ac.jp/EIC/EIC_News/105E.html

Kendrick, E., Bevis, M., Smalley Jr., R., Brooks, B., Vargas, R.B., Lauría, E., Fortes, L.P.S., 2003. The Nazca-South America Euler vector and its rate of change. J. S. Am. Earth Sci. 16 (2), 125–131. https://doi.org/10.1016/S0895-9811(03)00028-2

Kiser, E., Ishii, M., 2011. The 2010 Mw8.8 Chile earthquake: triggering on multi-ple segments and frequency-dependent rupture behavior. Geophys. Res. Lett. 38, L07301. http://dx.doi.org/10.1029/2011GL047140.

Kopp, H. 2013. Invited review paper: The control of subduction zone structural complexity and geometry on margin segmentation and seismicity. Tectonophysics 589, 1–16. http://dx.doi.org/10.1016/j.tecto.2012.12.037

Krabbenhoeft, A., Weinrebe, R.W., Kopp, H., Flueh, E.R., Ladage, S., Papenberg, C., Planert, L., Djajadihardja, Y., 2010. Bathymetry of the Indonesian Sunda marginrelating morphological features of the upper plate slopes to the location and extent of the seismogenic zone. Natural Haz. Earth Syst. 10, 1899-1911, https://doi.org/10.5194/nhess-10-1899-2010

Lamb, S., Davis, P., 2003. Cenozoic climate change as a possible cause for the rise of the Andes. Nature 425 (6960), 792-797. https://doi.org/10.1038/nature02049

Lange, D., Tilmann, F., Barrientos, S.E., Contreras-Reyes, E., Methe, P., Moreno, M., Heit, B., Agurto, H., Bernard, P., Vilotte, J.P., Beck, S., 2012. Aftershock seismicity of the 27 February 2010 Mw 8.8 Maule earthquake rupture zone. Earth Planet. Sci. Lett. 317-318, 413–425. https://doi.org/10.1016/j.epsl.2011.11.034

Lange, D., Geersen, J., Barrientos, S., Moreno, M., Grevemeyer, I., Contreras-Reyes, E., Kopp, H., 2016. Aftershock seismicity and tectonic setting of the 2015 September 16 Mw 8.3 Illapel earthquake, Central Chile. Geophys. J. Int. 206 (2), 1424-1430, https://doi.org/10.1093/gji/ggw218

Laske, G., Masters., G., Ma, Z. Pasyanos, M., 2013. Update on CRUST1.0 - A 1-degree Global Model of Earth's Crust. EGU General Assembly 2013. Geophys. Res. Abstr.. 15. EGU2013-2658.

Last, B.J., Kubik, K., 1983. Compact gravity inversion. Geophysics 48 (6), 713-721. https://doi.org/10.1190/1.1441501

Lay, T. 2015. The surge of great earthquakes from 2004 to 2014. Earth Planet. Sci. Lett. 409, 133-146. http://dx.doi.org/10.1016/j.epsl.2014.10.047

Lay, T., Kanamori, H., 1981. An asperity model of large earthquake sequences. In: Earthquake Prediction, An International Review, Volume 4, 579–592. Eds. Simpson, D.W., Richards, P.G., Maurice Ewing Book Series. https://doi.org/10.1029/ME004p0579

Lay, T., Bilek, S.L., 2007. Anomalous earthquake ruptures at shallow depths on subduction zone megathrusts. In: Dixon, T., Moore, J.C. (Eds.), The Seismogenic Zone of Subduction Thrust Faults. Columbia University Press, New York, pp. 476–511. ISBN: 9780231138666

Lay, T., Kanamori, H., Ruff, L., 1982. The asperity model and the nature of large subduction zone earthquakes. Earthquake Pred. Res. 1 (1), 3–71. ISSN 0286-0619. http://resolver.caltech.edu/CaltechAUTHORS:20150121-145948828

Lay, T., Ammon, C.J., Kanamori, H., Koper, K.D., Sufri, O., Hutko, A.R., 2010. Teleseismic inversion for rupture process of the 27 February 2010 Chile (Mw 8.8) earthquake. Earth Planet. Sci. Lett. 37, L1330 1. https://doi.org/I0.1029/201 OGL043379.

Lay, T., Kanamori, H., Ammon, C., Koper, K., Hutko, A., Ye, L., Yue, H., Rushing, T. 2012. Depth varying rupture properties of subduction zone megathrust faults. J. Geoph. Res., Solid Earth 117, B04311, https://doi.org/10.1029/2011JB009133

Lay, T., Yue, H., Brodsky, E.E., An, C., 2014. The 1 April 2014 Iquique, Chile, Mw 8.1 earthquake rupture sequence. Geophys. Res. Lett. 41, 3818-3825. http://dx.doi.org/10.1002/2014GL060238.

Li, X., 2001. Vertical resolution: Gravity versus vertical gravity gradient. The Leading Edge 20, 901-904. http://dx.doi.org/10.1190/1.1487304

Li, Y., Oldenburg, D.W., 1998. 3-D inversion of Gravity Data. Geophysics 63, 109-119. http://dx.doi.org/10.1190/1.1444302

Li, Y., Oldenburg, D.W., 1996. 3-D inversion of magnetic data. Geophysics 61, 394-408. http://dx.doi.org/10.1190/1.1443968

Llenos, A.L., Mc Guire, J.J., 2007. Influence of fore-arc structure on the extent of great subduction zone earthquakes. J. Geophys. Res., 112, B09301. http://dx.doi.org/10.1029/2007JB004944

Lomnitz, C., 2004. Major earthquakes of Chile: a historical survey, 1535-1960. Seismol. Res. Lett., 75, 368–378. http://dx.doi.org/10.1785/gssrl.75.3.368

Lorito, S., Romano, F., Atzori, S., Tong, X., Avallone, A., McCloskey, J., Cocco, M., Boschi, E., Piatanesi, A., 2011. Limited overlap between the seismic gap and coseismic slip of the great 2010 Chile earthquake. Nature Geosc. 4 (3), 173-177. https://doi.org/10.1038/ngeo1073

Loveless, J.P., Meade, B., 2011. Spatial correlation of interseismic coupling and coseismic rupture extent of the 2011MW=9.0 Tohoku-oki earthquake. Geophys. Res. Lett. 38 (17). https://doi.org/10.1029/2011GL048561

Loveless, J.P., Pritchard, M., Kukowski, N., 2010, Testing mechanisms of subduction zone segmentation and seismogenesis with slip distributions from recent Andean earthquakes. Tectonophysics 495, 1, 15-33. https://doi.org/10.1016/j.tecto.2009.05.008

Maksymowicz, A., Tréhuc, A.M., Contreras-Reyes, E., Ruiz, S., 2015. Density-depth model of the continental wedge at the maximum slip segment of the Maule Mw8.8 megathrust earthquake. Earth Planet. Sci. Lett. 409, 265-277. http://dx.doi.org/10.1016/j.epsl.2014.11.005

McGuire, J.J., Zhao, L., Jordan, T.H., 2002. Predominance of unilateral rupture for a global catalog of large earthquakes. Bull. Seismol. Soc. Am., 92, 3309-3317 http://dx.doi.org/10.1785/0120010293

Melgar, D., Fan, W., Riquelme, S., Geng, J., Liang, C., Fuentes, M., Vargas, G., Allen, R.M., Shearer, P.M., Fielding, E.J., 2016. Slip segmentation and slow rupture to the trench during the 2015, Mw8.3 Illapel, Chile earthquake. Geophys. Res. Lett. 43, 961-966, https://doi.org/10.1002/2015GL067369

Mendoza, C., Hartzell, S., Monfret, T., 1994. Wide band analysis of the 3 March 1985 central Chile earthquake: Overall source process and rupture history. Bull. Seism. Soc. Am. 84 (2), 269-283. https://pubs.geoscienceworld.org/ssa/bssa/article-abstract/84/2/269/119755/wide-band-analysis-of-the-3-march-1985-central?redirectedFrom=fulltext

Menke, W. 1984. Geophysical Data Analysis: Discrete Inverse Theory, 272 pp., Academic Press Inc., Fla. eBook ISBN: 9780323141284 https://doi.org/10.1016/B978-0-12-490920-5.X5001-7

Métois, M., Socquet, A., Vigny, C., 2012. Interseismic coupling, segmentation and mechanical behavior of the central chile subduction zone. J. Geophys. Res. 117 (B3), https://doi.org/10.1029/2011JB008736

Metois, M., Socquet, A., Vigny, C., Carrizo, D., Peyrat, S., Delorme, A., Maureira, E., Valderas-Bermejo, M.C., Ortega, I., 2013. Revisiting the North Chile seismic gap

segmentation using GPS-derived interseismic coupling. Geophys. J. Int. 194, 1283-1294. https://doi.org/10.1093/gji/ggt183

Métois, M., Vigny, C., Socquet, A., 2016. Interseismic coupling, megathrust earthquakes and seismic swarms along the Chilean subduction zone (38º-18ºS). Pure Appl. Geophys. 173, 1431. https://doi.org/10.1007/s00024-016-1280-5

Mochizuki, K., Yamada, T., Shinohara, M., Yamanaka, Y., Kanazawa, T., 2008. Weak interplate coupling by seamounts and repeating M~7 earthquakes. Science 321, 1194-1197. https://doi.org/10.1126/science.1160250

Molodensky, M.S., 1945. Main problem of geodetic gravimetry, Trans. Centr. Res. Inst. G, A & C 42, Geodezizdat, Moscow.

Molodensky, M.S., Eremeev, V.F., Yurkina,M.I., 1962. Methods for Study of the External Gravity Field and Figure of the Earth, Israel Program of Scientific Translations, Jerusalem (Russian original 1960).

Moreno, M., Rosenau, M., Oncken, O., 2010. 2010 Maule earthquake slip corre-lates with pre-seismic locking of Andean subduction zone. Nature 467, 198-202. http://dx.doi.org/10.1038/nature09349.

Moreno M., Melnick, D., Rosenau, M., Baez, J., Klotz, J., Oncken, O., Tassara, A., Chen, J., Bataille, K., Bevis, M., Socquet, A., Bolte, J., Vigny, C., Brooks, B., Ryder, I., Grund, V., Smalley, B., Carrizo, D., Bartsch, M., Hase, H., 2012. Toward understanding tectonic control on the Mw 8.8 2010 Maule Chile earthquake. Earth Planet. Sci. Lett. 321-322, 152-165. https://doi.org/10.1016/j.epsl.2012.01.006

Moreno, M., Haberland, C., Oncken, O., Rietbrock, A., Angiboust, S., Heidbach, O., 2014. Locking of the Chile subduction zone controlled by fluid pressure before the 2010 earthquake. Nature Geosc. 7, 292-296. https://doi.org/10.1038/NGEO2102

Müller, R.D., Landgrebe, T.C.W., 2012. The link between great earthquakes and the subduction of oceanic fracture zones. Solid Earth 3, 447-465. https://10.5194/se-3-447-2012

Nishenko, S. P., 1985. Seismic Potential for large and great interplate earthquakes along the Chilean and southern Peruvian margins of South America. A quantitative reappraisal. J. Geophys. Res. 90 (B5), 3589-3615. https://doi.org/10.1029/JB090iB05p03589

Norabuena, E., 2004. Space geodetic studies of crustal deformation in subduction zones: The central Andes and Costa Rica, Ph.D. thesis, 110 pp., Univ. of Miami, Coral Gables. https://search.proquest.com/openview/d478fa1dbfb5a02220dfce403739354d/1?pq-origsite=gscholar&cbl=18750&diss=y

Ozawa, S., Nishimura, T., Suito, H., Kobayashi, T., Tobita, M., Imakiire, T., 2011. Coseismic and postseismic slip of the 2011 magnitude-9 Tohoku-Oki earthquake. Nature 475 (0028-0836), 373-376. https://doi.org/10.1038/nature10227

Pail, R., Bruinsma, S., Migliaccio, F., Förste, C., Goiginger, H., Schuh, W.D., Höck, E., Reguzzoni, M., Brockmann, J.M., Abrikosov, O., Veicherts, M., Fecher, T., Mayrhofer, R., Krasbutter, I., Sansò, F., Tscherning, C.C., 2011. First GOCE gravity field models derived by three different approaches. J. Geod. 85, 819-843. https://doi.org/10.1007/s00190-011-0467-x

Pilkington, M., 1997. 3-D magnetic imaging using conjugate gradients. Geophysics 62, 1132-1142. http://dx.doi.org/10.1190/1.1826377

Pollitz, F.F., Brooks, B., Tong, X., Bevis, M.G., Foster, J.H., Bürgmann, R., Smalley, R.J., Vigny, C., Socquet, A., Ruegg, J.C., Campos, J., Barrientos, S., Parra, H., Baez Soto, J.C., Cimbaro, S., Blanco, M., 2011. Coseismic slip distribution of the February 27, 2010 Mw 8.8 Maule, Chile earthquake. Geophys. Res. Lett. 38 (L09309). https://doi.org/10.1029/2011GL047065

Pritchard, M.E., Norabuena, E.O., Ji, C., Boroschek, R., Comte, D., Simons, M., Dixon, T.H., Rosen, P.A., 2007. Geodetic, teleseismic, and strong motion constraints on slip from recent southern Peru subduction zone earthquakes. J. Geophys. Res. 112, B03307. https://doi.org/10.1029/ 2006JB004294

Ramos, V.A., 2010. The tectonic regime along the Andes: Present-day and Mesozoic regimes. Geol. J. 45, 2-25. https://doi.org/10.1002/gj.1193

Ramos, V.A., Folguera, A., 2009. Andean flat-slab subduction through time, in Murphy, J.B., Keppie, J.D., and Hynes, A.J., eds., Ancient Orogens and Modern Analogues: Geol. Soc. London Spec. Pub. 327, 31-54. http://dx.doi.org/10.1144/SP327.3

Ranero C.R., von Huene R., Weinrebe W., Reichert C., 2006. Tectonic Processes along the Chile Convergent Margin. In: Oncken O. et al. (eds) The Andes - Active Subduction

Orogeny. Frontiers in Earth Sciences. Springer, Berlin, Heidelberg. pp 91-121. https://doi.org/10.1007/978-3-540-48684-8_5

Robinson, D.P., Das, S., Watts, A.B., 2006. Earthquake rupture stalled by a subducting fracture zone. Science 312, 1203-1205, https://doi.org/10.1126/ science.1125771

Rosenbaum, G., Giles, D., Saxon, M., Betts, P.G., Weinberg, R.F., Duboz, C., 2005. Subduction of the Nazca Ridge and the Inca Plateau: Insights into the formation of ore deposits in Peru. Earth Planet. Sci. Lett. 239 (1-2), 18-32. https://doi.org/10.1016/j.epsl.2005.08.003

Rubin, A. M., Gillard, D., 2000. Aftershock asymmetry/rupture directivity among central San Andreas fault microearthquakes, J. Geophys. Res. 105, 19,095-19,109. https://doi.org/10.1029/2000JB900129

Ruegg J.C., Olcay, M., Lazo, D., 2001. Co-, Post- and Pre(?)-seismic Displacements Associated with the Mw8.4 Southern Peru Earthquake of 23 June 2001 from Continuous GPS Measurements. Seism. Res. Lett. 72 (6), 673-678. https://doi.org/10.1785/gssrl.72.6.673

Ruff, L.J., 1989. Do trench sediments affect great earthquake occurrence in subduction zones? Pure App. Geophys. 129, 263-282. https://doi.org/10.1007/BF00874629

Ruiz, S., Metois, M., Fuenzalida, A., Ruiz, J., Leyton, F., Grandin, R., Vigny, C., Madariaga, R., Campos, J., 2014. Intense foreshocks and a slow slip event preceded the 2014 Iquique Mw=8.1 earthquake. Science 345, 6201, 1165-1169. https://doi.org/10.1126/science.1256074

Rummel, R., Yi, W., Stummer, C., 2011. GOCE gravitational gradiometry, J. Geodyn. 85 (11), 777-790. https://doi.org/10.1007/s00190-011-0500-0

Salichon, J., Delouis, B., Lundgren, P., Giardini, D., Costantini, M., Rosen, P., 2003. Joint inversion of broadband teleseismic and interferometric synthetic aperture radar (InSAR) data for the slip history of the Mw = 7.7, Nazca ridge (Peru) earthquake of 12 November 1996. J. Geophys. Res. 108 (B2), 2085. https://doi.org/10.1029/2001JB000913

Sallares, V., Ranero, C. R., 2005. Structure of the North Chile erosional convergent margin off Antofagasta (23º30'S). J. Geophys. Res. 110 (B6). https://doi.org/10.1029/2004JB003418

Schurr, B., Asch, G., Hainzl, S., Bedford, J., Hoechner, A., Palo, M., Wang, R., Moreno, M., Bartsch, M., Zhang, Y., Oncken, O., Tilmann, F., Dahm, T., Victor, P., Barrientos, S., Vilotte, J.P., 2014. Gradual unlocking of plate boundary controlled initiation of the 2014 Iquique earthquake. Nature 512, 299-302. https://doi.org/10.1038/nature13681

Shrivastava, M.N., González, G., Moreno, M., Chlieh, M., Salazar, P., Reddy, C.D., Báez, J.C., Yáñez, G., González, J., de la Llera, J.C., 2016. Coseismic slip and afterslip of the 2015 Mw 8.3 Illapel (Chile) earthquake determined from continuous GPS data. Geophys. Res. Lett. 43. https://doi.org/10.1002/2016GL070684

Smith, W.H.F., Sandwell, D.T., 1997. Global seafloor topography from satellite altimetry and ship depth soundings. Science 277 (5334), 1956-1962. https://doi.org/10.1126/science.277.5334.1956

Sobiesiak, M.M., Meyer, U., Schmidt, S., Götze, H.J., Krawczyk, C., 2007. Asperity generating upper crustal sources revealed by b-value and isostatic residual anomaly grids in the area of Antofagasta. J. Geophys. Res. 112, B12308. https://doi.org/10.1029/2006JB004796

Socquet, A., Valdes, J.P., Jara, J., Cotton, F., Walpersdorf, A., Cotte, N., Specht, S., Ortega-Culaciati, F., Carrizo, D., Norabuena, E., 2017. An 8 month slow slip event triggers progressive nucleation of the 2014 Chile megathrust. Geophys. Res. Lett., 44, 4046-4053, https://doi.org/10.1002/2017GL073023

Song, T.R., Simons, M., 2003. Large trench-parallel gravity variations predict seismogenic behavior in subduction zones. Science 301, Issue 5633, 630-633. https://doi.org/10.1126/science.1085557

Spagnotto, S., Alvarez, O., Folguera, A. 2018. Static Stress Increase in the Outer Forearc Produced by MW 8.2 September 8, 2017 Mexico Earthquake and its Relation to the Gravity Signal. Pure App. Geophys. 175 (8), 2575-2593. https://doi.org/10.1007/s00024-018-1962-2

Sparkes, R., Tilmann, F., Hovius, N., Hillier, J., 2010. Subducted seafloor relief stops rupture in South American great earthquakes: Implications for rupture behavior in the 2010 Maule, Chile earthquake. Earth Planet. Sci. Lett. 298, 89-94. https://doi.org/10.1016/j.epsl.2010.07.029

Sugiyama, Y., 1994. Neotectonics of southwest Japan due to the right-oblique subduction of the Philippine Sea plate. Geofis. Int. 33 (1), 53-76. http://dx.doi.org/10.22201/igeof.00167169p.1994.33.1.540

Swenson, J. L., Beck, S.L., 1996. Historical 1942 Ecuador and 1942 Peru subduction earthquakes, and earthquake cycles along Colombia-Ecuador and Peru subduction segments. Pure Appl. Geophys. 146 (1), 67– 101. https://doi.org/10.1007/BF00876670

Swenson, J. L., Beck, S.L., 1999. Source characteristics of the 12 November 1996 Mw 7.7 Peru subduction zone earthquake. Pure Appl. Geophys. 154 (3), 731-751, https://doi.org/10.1007/s000240050250

Tassara, A., 2010. Control of forearc density structure on megathrust shear strength along the Chilean subduction zone. Tectonophysics 495, 34-47. https://doi.org/10.1016/j.tecto.2010.06.004

Tavera, H., Fernandez, E., Bernal, I., Antayhua, Y., Aguero, C., Salas, H., Rodriguez, S., Vilcapoma, L., Zamudio, Y., Portugal, D., Inza, A., Carpio, J., Ccallo, F., Valdivia, I., 2006. The southern region of Peru earthquake of June 23rd, 2001. J. Seismol. 10 (2), 171-195. https://doi.org/10.1007/s10950-006-9014-2

Tilmann, F., Zhang, Y., Moreno, M., Saul, J., Eckelmann, F., Palo, M., Deng, Z., Babeyko, A., Chen, K., Baez, J.C., Schurr, B., Wang, R., Dahm, T. (2016), The 2015 Illapel earthquake, central Chile: A type case for a characteristic earthquake? Geophys. Res. Lett. 43, 574-583. https://doi.org/10.1002/2015GL066963

Tong, X., Sandwell, D., Luttrell, K., Brooks, B., Bevis, M., Shimada, M., Foster, J., Smalley Jr., R., Parra, H., Soto, J.C.B., Blanco, M., Kendrick, E., Genrich, J., Caccamise II, D.J., 2010. The 2010 Maule, Chile earthquake: downdip rupture limit revealed by space geodesy. Geophysi. Res. Lett. 37. https://doi.org/10.1029/2010GL045805

Tscherning, C.C., 1976. Computation of the second-order derivatives of the normal potential based on the representation by a Legendre series, Manuscripta Geodaetica, 1(1), 71-92.

Uieda, L., Barbosa, V.C.F., 2017. Fast nonlinear gravity inversion in spherical coordinates with application to the South American Moho. Geophys. J. Int. 208, 162-176. https://doi.org/10.1093/gji/ggw390

Uieda, L., Ussami, N., Braitenberg, C.F., 2010. Computation of the gravity gradient tensor due to topographic masses using tesseroids.Eos Trans. AGU, 91 (26).Meeting America Supply, Abstract G22A-04. World Wide Web Address: http://code.google.com/p/tesseroids/

Uieda, L., Barbosa, V., Braitenberg, C., 2016. Tesseroids: Forward-modeling gravi-tational fields in spherical coordinates. Geophysics 81 (5), F41–F48, https://doi.org/10.1190/geo2015-0204.1

Vigny, C., Socquet, A., Peyrat, S., Ruegg, J.C., Métois, M., Madariaga, R., Morvan, S., Lancieri, M., Lacassin, R., Campos, J., Carrizo, D., Bejar-Pizarro, M., Barrientos, S., Armijo, R., Aranda, C., Valderas-Bermejo, M.-C., Ortega, I., Bondoux, F., Baize, S., Lyon-Caen, H., Pavez, A., Vilotte, J.P., Bevis, M., Brooks, B., Smalley, R., Parra, H., Baez, J.-C., Blanco, M., Cimbaro, S., Kendrick, E., 2011. The 2010 *Mw* 8.8 Maule megathrust earthquake of Central Chile, monitored by GPS. Science 332 (6036), 1417-1421. https://doi.org/10.1126/science.1204132

Völker, D., Wiedicke, M., Ladage, S., Gaedicke, C., Reichert, C., Rauch, K., Kramer, W., Heubeck, C., 2006. Latitudinal Variation in Sedimentary Processes in the Peru-Chile Trench off Central Chile. In: Oncken O. et al. (eds) The Andes - Active Subduction Orogeny. Frontiers in Earth Sciences, Part II. Springer, Berlin, Heidelberg. pp 193-216. https://doi.org/10.1007/978-3-540-48684-8_9ç

von Huene, R., Scholl, D.W., 1991. Observations at convergent margins concerning sediment subduction, subduction erosion, and the growth of continen tal crust. Rev Geophys. 29, 279-316. https://doi.org/10.1029/91RG00969

von Huene, R., Miller, J.J., Weinrebe, W., 2012. Subducting plate geology in three great earthquake ruptures of the western Alaska margin, Kodiak to Unimak. Geosphere 8 (3), 628–644. https://doi.org/10.1130/GES00715.1

Wang, K., Bilek, S., 2011. Do subducting seamounts generate or stop large earthquakes? Geology 39, 819-822. https://doi.org/10.1130/G31856.1

Wang, K., Bilek, S.L., 2014. Invited review paper: Fault creep caused by subduction of rough seafloor relief. Tectonophysics 610, 1-24. https://doi.org/10.1016/j.tecto.2013.11.024.

Wells, R.E., Blakely, R.J., Sugiyama, Y., Scholl, D.W., Dinterman, P.A., 2003. Basin centered asperities in great subduction zone earthquakes: a link between slip, subsidence and subduction erosion? J. Geophys. Res. 108 (B10), 2507–2536. http://dx.doi.org/10.1029/2002JB002072.

Whittaker, J., Goncharov, A., Williams, S., Müller, R.D, Leitchenkov, G., 2013. Global sediment thickness dataset updated for the Australian-Antarctic Southern Ocean. Geochem. Geophys. Geosystems 14, 3297-3305. https://doi.org/10.1002/ggge.20181

Wild-Pfeiffer, F., 2008. A comparison of different mass element for use in gravity gradiometry. J. Geod. 82, 637-653. https://doi.org/10.1007/s00190-008-0219-8

Ye, L., T. Lay, H. Kanamori, Rivera, L., 2016a. Rupture characteristics of major and great (Mw ≥ 7.0) megathrust earthquakes from 1990 to 2015: 1. Source parameter scaling relationships. J. Geophys. Res. Solid Earth 121. https://doi.org/10.1002/2015JB012426

Ye, L., T. Lay, H. Kanamori, Rivera, L., 2016b. Rupture characteristics of major and great (Mw ≥ 7.0) megathrust earthquakes from 1990 to 2015: 2. Depth dependence. J. Geophys. Res. Solid Earth 121. https://doi.org/10.1002/2015JB012427.

Zhdanov, M. S. 2002. Geophysical Inverse Theory and Regularization Problems, Methods in Geochemistry and Geophysics, vol. 36, 668 pp., Elsevier Science. eBook ISBN: 9780080532509

Figures Legends:

Figure 1: ***Up:*** *Shaded relief map of the Nazca-South American plates from ETOPO1 (Amante and Eakins, 2009) with main bathymetric features. Orange dashed ellipses indicate locations of the main areas displayed in Figs. 2–10 for the last Mw>8.0 earthquakes along the Peru-Chilean margin.* ***References: A)*** *2001 Mw=8.4 Arequipa earthquake,* ***B)*** *2010 Mw=8.8 Maule earthquake,* ***C:*** *2015 Mw=8.3 Illapel earthquake,* ***D:*** *2014 Mw=8.4 Pisagua-Iquique earthquake.* ***Down:*** *Schematic cross-section explaining rupture domains of megathrust rupture characteristics from Lay et al. (2012).* ***Domain A*** *is located close to the trench where tsunami earthquakes or anelastic deformation and stable sliding occur. The central megathrust "****domain B"*** *is where large earthquakes and high slip occurs with minor short-period seismic radiation along large and relatively uniform regions with unstable sliding frictional properties (asperities). Downdip is located* ***domain***

C *were moderate slip occurs along patchy smaller scale regions of stable sliding surrounded by conditionally stable areas. The transitional* ***domain D*** *where slow slip events, low frequency earthquakes, and seismic tremor can occur is only present in some areas around the world.* ***References:*** *grey shaded ellipse in Domain A represent sediments and pore fluids at shallow depths. Dark shaded irregular bodies* labeled "seismic" are regions that present unstable frictional sliding. *Small, isolated patches may behave as "repeaters" when quasi-static sliding of surrounding regions regularly load them to failure. Thick black dotted line represents the interplate megathrust fault. For more details see Lay et al. (2012).*

Figure 2: *Topography and sediment corrected vertical gravity gradient in the Central Andes and adjacent Nazca plate, obtained from GOCE satellite-only model GO_CONS_GCF_2_DIR_R5 (Bruinsma 2013),* **A:** *up to N=300. In the right corner is shown in detail the landslide scar with white solid lines (Smith and Sandwell, 1997; Amante and Eakins 2009; Audin et al. (2008) and the Chololo Fault System with blue solid line.* **B:** *up to N=250. In the right corner is shown the enlarged forearc area were slip increased in a region of relative minima Tzz. A similar pattern is highlighted at the SE ending of the rupture (dashed red circle).* ***C:*** *up to N=200. The +5 Eötvös contour (thick black line) depicts higher densities to the NW and SE of the epicenter along the forearc. A low Tzz anomaly to the SSE of the epicenter connects to the maximum slip, following the rupture propagation in the southward direction (blank white arrow).* ***D:*** *Topography and sediment corrected residual gravity disturbance in the Central Andes and adjacent Nazca plate, obtained from GOCE satellite-only model GO_CONS_GCF_2_DIR_R5 (Bruinsma 2013) up to N=300-10. Red dashed line indicates profile of Fig. 11A.* ***References:*** *Nazca-South American plates convergence (white arrow) is from Kendrick et al. (2003), the Perú-Chilean trench is indicated with a gray dashed line. Supperimposed slip distribution (orange solid line) for the 2001 Mw=8.4 Arequipa earthquake (Chlieh et al. 2011). Red star indicates the epicenter.*

Figure 3: *Topography and sediment corrected Tzz slices calculated at different degrees of the harmonic expansion. Degree orders between N=200 to 300 depict anomalies at approximate depths of the seismogenic zone (interplate contact), while higher degrees as N=175 and N=150 show the effect of the oceanic plate.* ***References:*** *black dashed ellipses*

indicates main asperities of region B, white dashed ellipse indicate minor asperities in region C, black dotted ellipses indicate the location of seismic barriers, white blank arrow indicates rupture propagation direction.

Figure 4: *Topography and sediment corrected vertical gravity gradient in the region of Maule earthquake, obtained from GOCE satellite-only model GO_CONS_GCF_2_DIR_R5 (Bruinsma 2013),* **A:** *up to N=300.* **B:** *up to N=250. Superimposed are the Lanalhue (LF) and Pichilemu (PF) major upper plate faults (grey dashed lines) from Moreno et al (2012). The upper continental forearc (Cf), the 40 km wide and 20 km thick Cobquecura anomaly (CA), and the smaller Pichilemu anomaly (PA) lying above the plate interface (at 25km depth) were taken from Hicks et al (2012).* ***C:*** *up to N=200. The -5 Eötvös contour (thick black line) roughly coincide with the seismogenic zone along the forearc. The -10 Eötvös contour coincides with the location of maximum slip lobes. Solid white arrows indicate a narrowing of the Tzz minima contours which corresponds to slip ending. White dashed lines are major upper plate faults from Moreno et al (2012): Thrust Ridge (TR), Santa María Fault (SMF), Lanalhue Fault (LF) and Pichilemu Fault (PF).* ***D:*** *Topography and sediment corrected residual gravity disturbance obtained from GOCE satellite-only model GO_CONS_GCF_2_DIR_R5 (Bruinsma 2013) up to N=300-10. Red dashed line indicates profile of Fig. 11B. Dashed ellipse contours a shelf basin from Maksymowiccz et al. (2015).* ***References:*** *Nazca-South American plates convergence (black arrow) is from DeMets et al. (2010), the Perú-Chilean trench is indicated with a gray dashed line. Supperimposed slip distribution (orange solid line) for the 2010 Mw=8.8 Maule (Moreno et al. 2012) earthquake. Red star indicates the epicenter.*

Figure 5: *Topography and sediment corrected Tzz slices calculated at different degrees of the harmonic expansion. Degree orders between N=200 to 300 depict anomalies at approximate depths of the seismogenic zone (interplate contact), while higher degrees as N=175 and N=150 show the effect of the oceanic plate. The minima Tzz lobe to the north could be related to a higher dip angle of the slab as reported by Moreno et al. (2012).* ***References:*** *black dashed ellipses indicates main asperities of region B, white dashed ellipse indicate minor asperities in region C, black dotted contours indicate the location of seismic barriers, white blank arrow indicates rupture propagation direction.*

Figure 6A: *Topography and sediment corrected vertical gravity gradient in the region of Illapel earthquake, obtained from GOCE satellite-only model GO_CONS_GCF_2_DIR_R5 (Bruinsma 2013) up to N=300.* ***B:*** *Topography and sediment corrected residual gravity disturbance obtained from GOCE satellite-only model GO_CONS_GCF_2_DIR_R5 (Bruinsma 2013) up to N=300-10. Red dashed line indicates profile of Fig. 11C. Blue dashed lines indicate inflections of the +50 mGal and +25 mGal contours related to these oceanic features. Slip increases inland over a* ***Gd*** *relative minima lobe.* ***References:*** *solid orange contours indicate the slip distribution for the 2015 Mw=8.3 Illapel earthquake (Tilmann et al. 2016), red star indicates the epicenter. Nazca-South American plates convergence (white arrow) is from DeMets et al. (2010), the Perú-Chilean trench is indicated with a gray dashed line, white dashed lines are approximate to the extrapolation of the CFZ and JFR beneath the continent.*

Figure 7: *Topography and sediment corrected Tzz slices calculated at different degrees of the harmonic expansion. Degree orders between N=200 to 300 depict anomalies at approximate depths of the seismogenic zone (interplate contact), while higher degrees as N=175 and N=150 show the effect of the oceanic plate as the inception points of the CFZ and the JFR.* ***References:*** *black dashed ellipses indicates main asperities of region B, white dashed ellipse indicate minor asperities in region C, black dotted contours indicate the location of seismic barriers, white blank arrow indicates rupture propagation direction.*

Figure 8: *Topography corrected vertical gravity gradient in the region of Pisagua earthquake, obtained from GOCE satellite-only model GO_CONS_GCF_2_DIR_R5 (Bruinsma 2013) between N=150 and N=300. Nazca-South American plates convergence (black arrow) is from DeMets et al. (2010) (the Perú-Chilean trench is indicated with a gray dashed line. Supperimposed slip distribution for the 2014 Mw=8.4 Pisagua-Iquique earthquake from a joint inversion (Schurr et al. 2014). Red star indicates the epicenter. At degrees between 150<N<200 a high tzz signal matches rupture and foreshocks sequence. This suggests that the IR subduction played a key role in rupture process as suggested by other authors (e.g. Geersen et al. 2017).*

Figure 9: *Topography and sediment corrected Tzz slices calculated at different degrees of the harmonic expansion. Minimum Tzz lobe dissipates as depth increases (N>200) giving place to a high gradient signal in the region where foreshocks sequence and rupture*

occurred. For N=225, rupture roughly coincides with minimum Tzz lobe and relative Tzz highs at rupture endings, which could be indicative of seismic barriers. ***References:*** *black dashed ellipses indicates main asperities of region B, white dashed ellipse indicate minor asperities in region C, black dotted ellipses indicate the location of seismic barriers, white blank arrow indicates rupture propagation direction.*

Figure 10: *Topography and sediment corrected residual gravity disturbance obtained from GOCE satellite-only model GO_CONS_GCF_2_DIR_R5 (Bruinsma 2013) up to N=300-10. Red dashed line indicates profile of Fig. 11D. Opposite to that observed for the other events, the rupture area coincides with a relative maximum of the gravity signal.*

Figure 11: *Inversion models along 2D sections of the topography and sediments corrected residual gravity disturbances (see Figs. 2D, 4D, 6B and 10 for location on profiles).* **A:** *For the 2001 Mw=8.4 Arequipa earthquake maximum slip occurred over minimum Gd. Low density contrast along both plates is interpreted as due to a marine forearc basin caused by upper plate bending related to the subduction of the Nazca Fz.* **B:** *for the 2010 Mw=8.8 Maule earthquake maximum slip occurred over minimum Gd. Subducted plane inflection between 34ºS and 36ºS is from Moreno et al. (2012).* **C:** *for the 2015 Mw=8.3 Illapel earthquake Slip is confined between two high-density regions along strike, related to subducted high oceanic features.* **D:** *for the Pisagua earthquake slip nucleated to the south of the higher density contrast to the north related to a subducted seamount.*

Figure 12: *Schematic interpretation of vertical gravity gradient from GOCE and its relation to rupture area. Low Tzz lobes between the trench and the coastline are indicating the location of seismic asperities in the "Domain B" from Lay et al. (2012); these low Tzz lobes are related to regions with a high slip, higher degree of seismic coupling and to marginal basins. The along strike segmentation (white dashed lines) is marked by a narrowing of the signal along the marine forearc, this along strike segmentation coincides whth regions of intermediate to low degree of seismic coupling (Metois et al. 2016). Beneath the coastline high Tzz values are indicating anomalous regions (with a higher density and high Vp) acting as across strike seismic barriers (close to the downdip limit of the seismogenic zone). Low Tzz values along the continental forearc (close to the coastline) coincide with regions were slip increased and with lower Vp (Hicks et al. 2014). These low*

Tzz anomalies are probably indicating the location of seismic asperities typical of "Domain C" from Lay et al. (2012).

Table 1: *Associated depth (Z_l) of a causative mass with a determined degree of the spherical harmonic expansion for* ***Tzz****.*

Table 2: *Parameters, restrictions and statistics for the different models: D (profile distance), Z (depth of the model), ncel (nº of blocks in the x and y directions), B factor, range of density variation, number of iterations until convergence of the solution, RMS error and ratio reduction.*

Degree/Order N	***Spatial resolution*** $\lambda/2=\pi R/N_{max}$ ***[Km]***	Z_l***[Km] for*** Δ_g ***(Featherstone 1997)***	Z_l***[Km] for Tzz*** (H_c***=7km)***
300	66.72	21.31	20.98
275	72.78	23.251	22.86
250	80.06	25.581	25.11
225	88.95	28.441	27.85
200	100.07	32.011	31.26
175	114.37	36.611	35.62
165	121.3	38.84	37.73
150	133.43	42.76	41.40
125	160.12	51.38	49.42
100	200.15	64.35	61.29

Table 1: *Associated depth (Z_l) of a causative mass with a determined degree of the spherical harmonic expansion for* ***Tzz****.*

Profile	**D** ***(km)***	**Z** ***(km)***	**ncel$_x$**	**ncel$_y$**	**B**	ρ_{min} ***(Kg/m^3)***	ρ_{max} ***(Kg/m^3)***	**Nº it**	**RMS** ***(mGal)***	**Ratio**
Arequipa	460	25	46	25	0.9	-50	75	14	0.214066	0.005560
Maule	580	25	58	25	0.95	-75	75	6	0.085989	0.058921
Illapel	270	25	54	25	0.95	-50	200	44	0.171580	0.009714
Pisagua	280	25	28	25	0.9	-50	200	34	0.461098	0.009814

Table 2: *Parameters, restrictions and statistics for the different models: D (profile distance), Z (depth of the model), ncel (nº of blocks in the x and y directions), B factor, range of density variation, number of iterations until convergence of the solution, RMS error and ratio reduction.*

Highlights

- Slip behavior along the Chilean margin is highly related to the density structure
- GOCE signal allows mapping along and across strike heterogeneities and directivity
- This method allows determining regions with higher seismic hazard along the margin
- Satellite GOCE data allows mapping physical properties along the plate interface

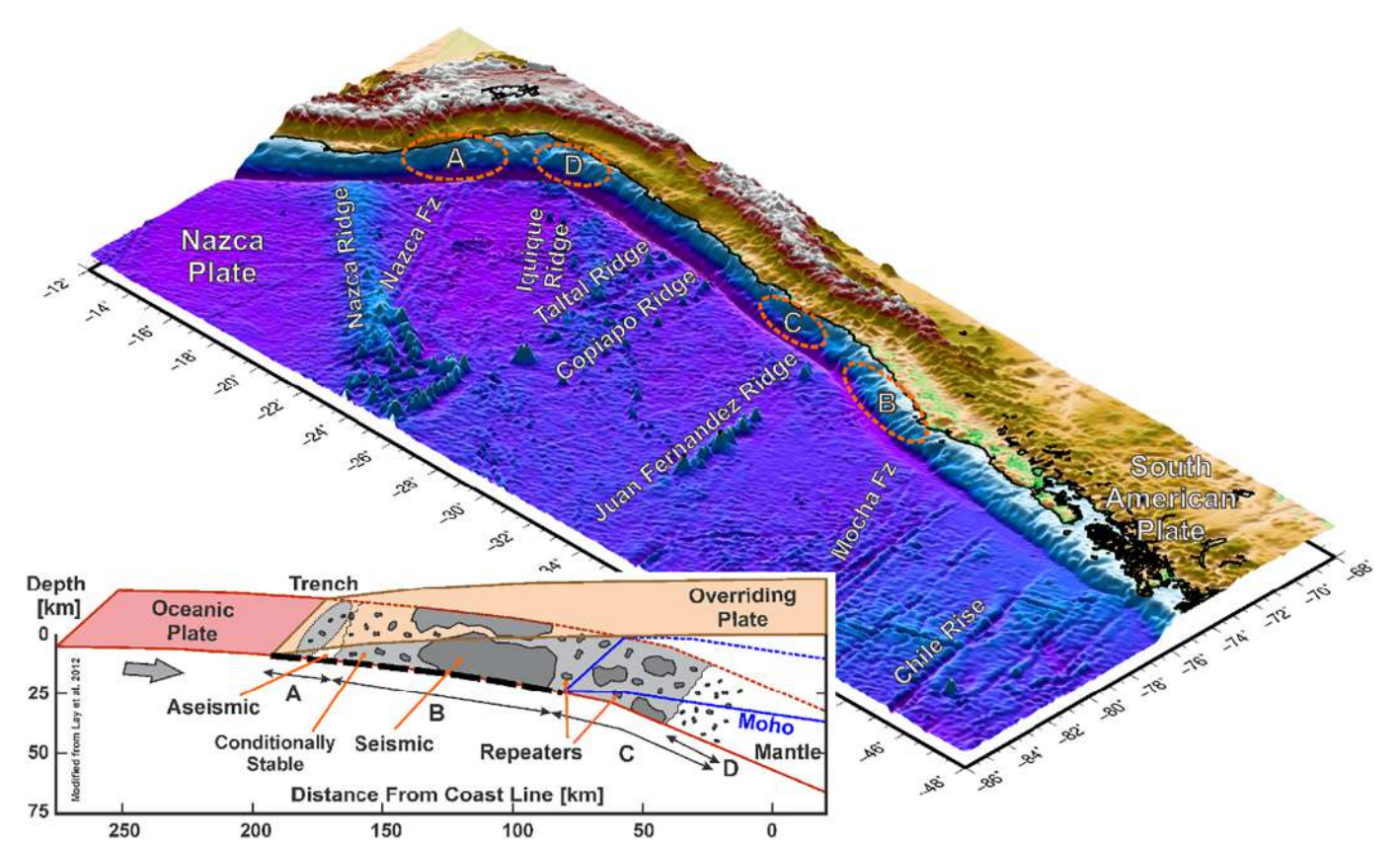
Nazca Plate
Nazca Ridge
Nazca Fz
Iquique Ridge
Taltal Ridge
Copiapo Ridge
Juan Fernandez Ridge
Mocha Fz
Chile Rise
South American Plate
A
B
C
D
Depth [km]
Trench
Oceanic Plate
Overriding Plate
Aseismic
Conditionally Stable
Seismic
Repeaters
Moho
Mantle
Distance From Coast Line [km]
Modified from Lay et al. 2012

Figure 1

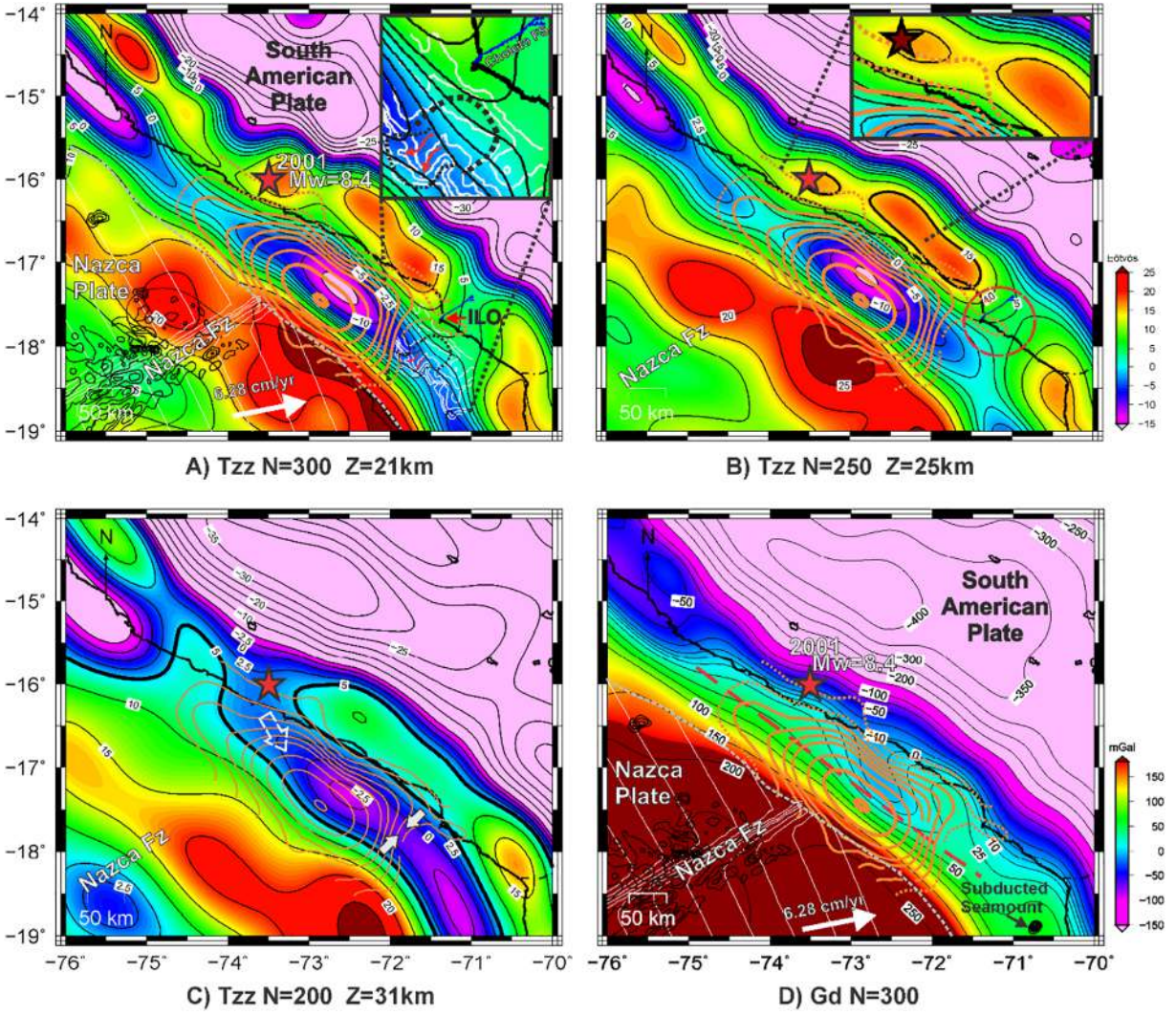
South American Plate
2001 Mw=8.4
Nazca Plate
Nazca Fz
6.28 cm/yr
50 km
ILO
A) Tzz N=300 Z=21km
B) Tzz N=250 Z=25km
C) Tzz N=200 Z=31km
D) Gd N=300
2001 Mw=8.4
Subducted Seamount
Eötvös
mGal
−14°
−15°
−16°
−17°
−18°
−19°
−76°
−75°
−74°
−73°
−72°
−71°
−70°

Figure 2

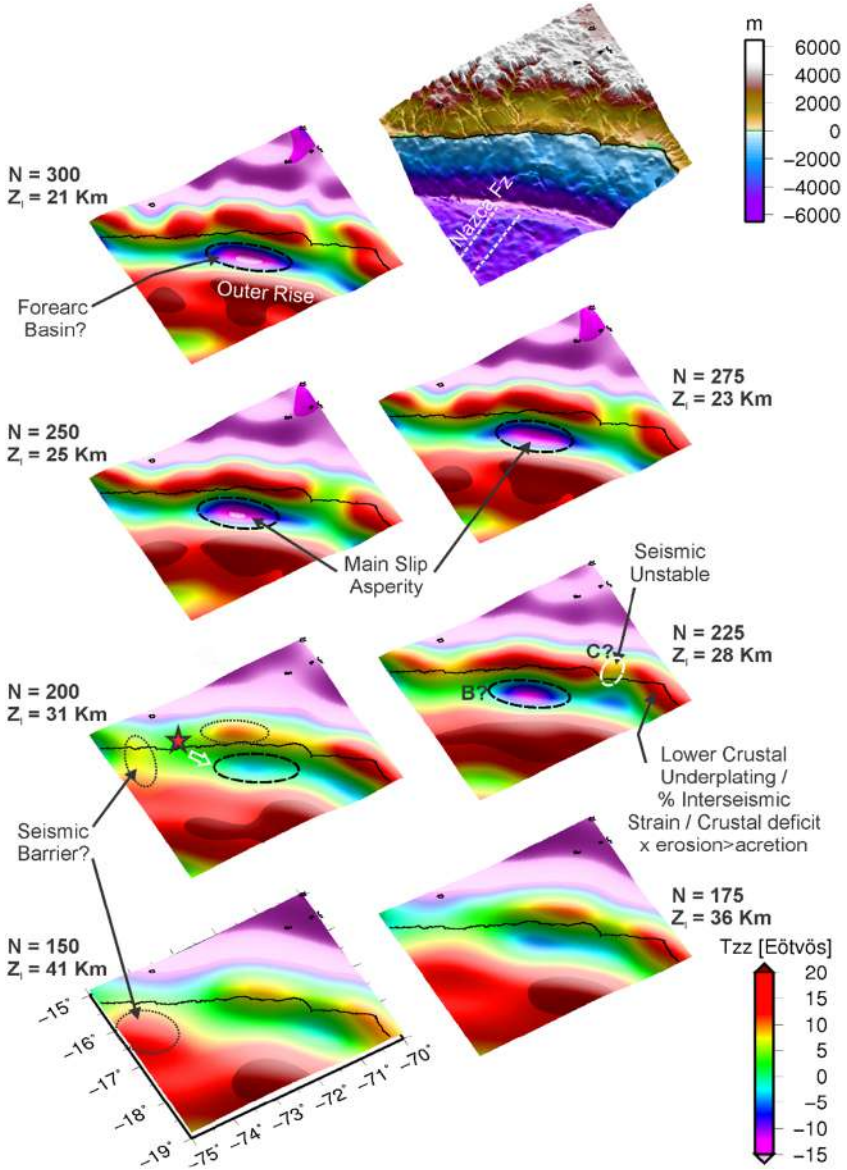
m
6000
4000
2000
0
−2000
−4000
−6000
Nazca FZ
N = 300
Z = 21 Km
Outer Rise
Forearc
Basin?
N = 275
Z = 23 Km
N = 250
Z = 25 Km
Main Slip
Asperity
Seismic
Unstable
C?
N = 225
Z = 28 Km
B?
N = 200
Z = 31 Km
Lower Crustal
Underplating /
% Interseismic
Strain / Crustal deficit
x erosion>acretion
Seismic
Barrier?
N = 175
Z = 36 Km
N = 150
Z = 41 Km
Tzz [Eötvös]
20
15
10
5
0
−5
−10
−15
−15°
−16°
−17°
−18°
−19°
−75°
−74°
−73°
−72°
−71°
−70°

Figure 3

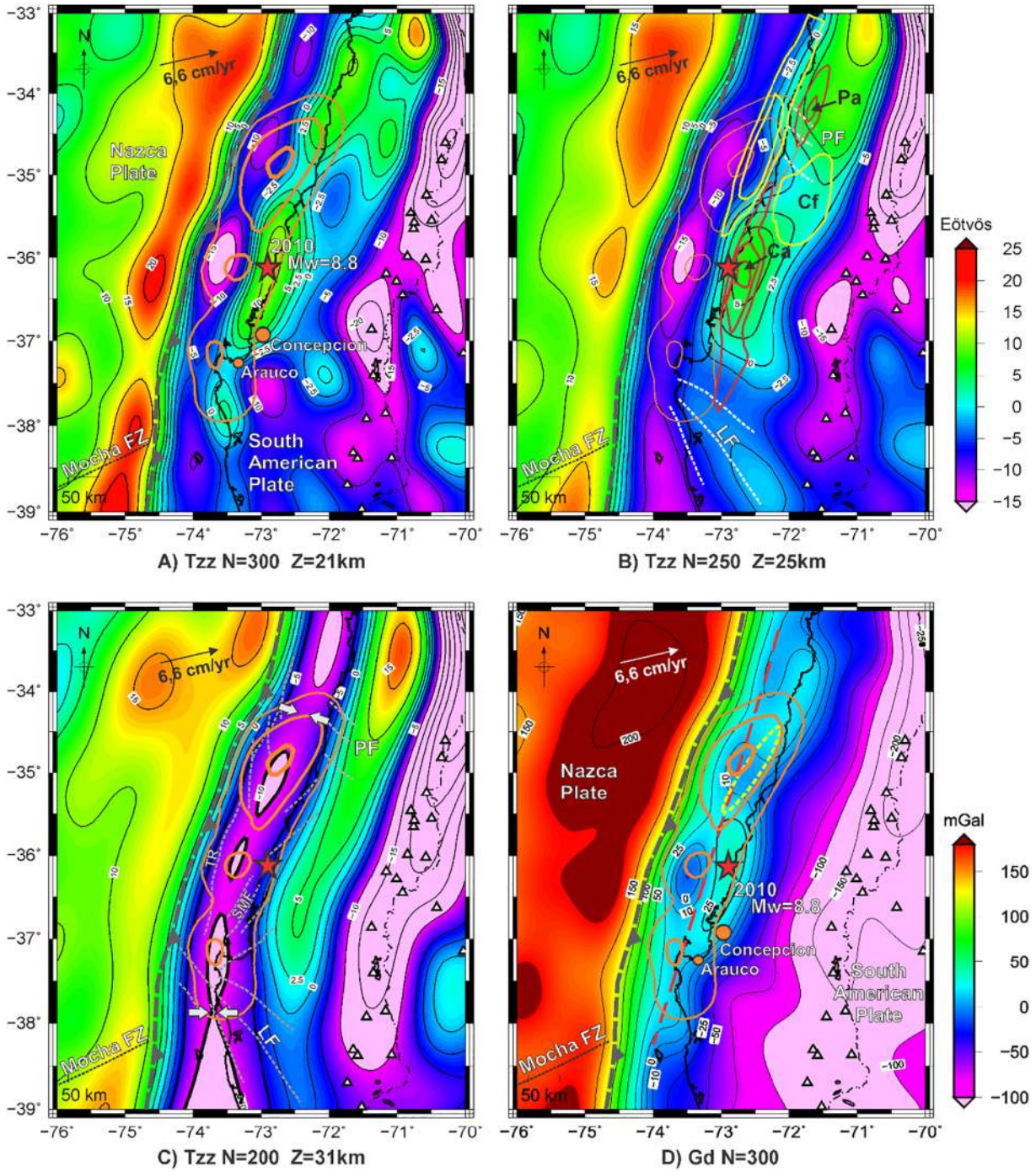
N
6,6 cm/yr
Nazca Plate
2010 Mw=8.8
Concepcion
Arauco
South American Plate
Mocha FZ
50 km
A) Tzz N=300 Z=21km
Pa
PF
Cf
Ca
LF
B) Tzz N=250 Z=25km
Eötvös
25
20
15
10
5
0
−5
−10
−15
IR
SMF
C) Tzz N=200 Z=31km
D) Gd N=300
mGal
150
100
50
0
−50
−100
−33°
−34°
−35°
−36°
−37°
−38°
−39°
−76°
−75°
−74°
−73°
−72°
−71°
−70°

Figure 4

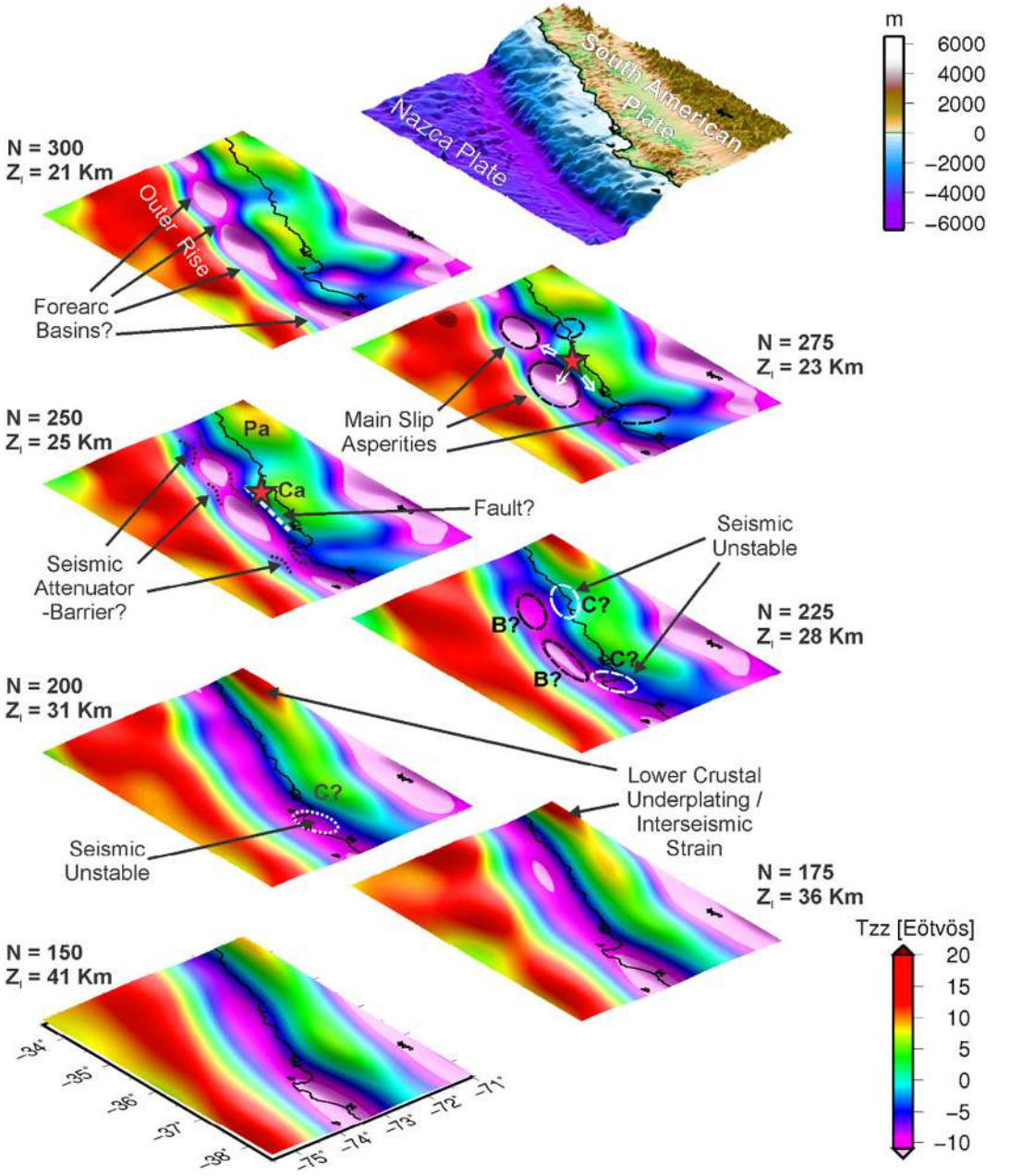
m
6000
4000
2000
0
−2000
−4000
−6000
South American Plate
Nazca Plate
N = 300
Z = 21 Km
Outer Rise
Forearc Basins?
N = 275
Z = 23 Km
Main Slip Asperities
N = 250
Z = 25 Km
Pa
Ca
Fault?
Seismic Attenuator -Barrier?
Seismic Unstable
C?
B?
C?
B?
N = 225
Z = 28 Km
N = 200
Z = 31 Km
C?
Seismic Unstable
Lower Crustal Underplating / Interseismic Strain
N = 175
Z = 36 Km
N = 150
Z = 41 Km
−34°
−35°
−36°
−37°
−38°
−75°
−74°
−73°
−72°
−71°
Tzz [Eötvös]
20
15
10
5
0
−5
−10

Figure 5

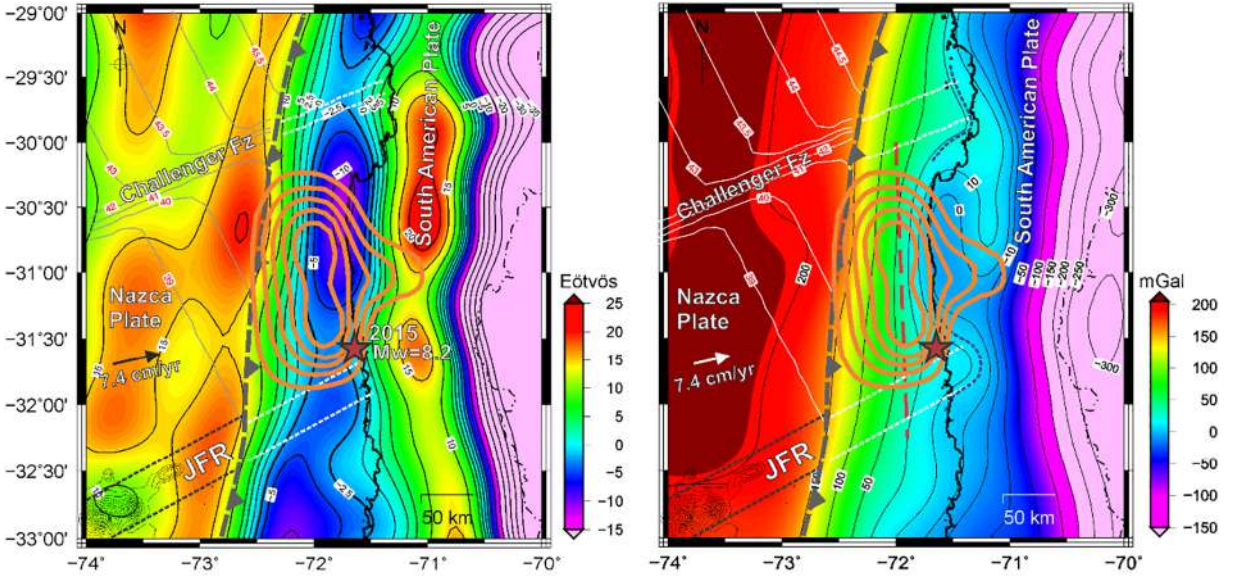
Challenger Fz
South American Plate
Nazca Plate
7.4 cm/yr
JFR
2015
Mw=8.2
50 km
Eötvös
25
20
15
10
5
0
−5
−10
−15
−29°00'
−29°30'
−30°00'
−30°30'
−31°00'
−31°30'
−32°00'
−32°30'
−33°00'
−74°
−73°
−72°
−71°
−70°
A) Tzz N=300 Z=21km
Challenger Fz
South American Plate
Nazca Plate
7.4 cm/yr
JFR
50 km
mGal
200
150
100
50
0
−50
−100
−150
−74°
−73°
−72°
−71°
−70°
B) Gd N=300

Figure 6

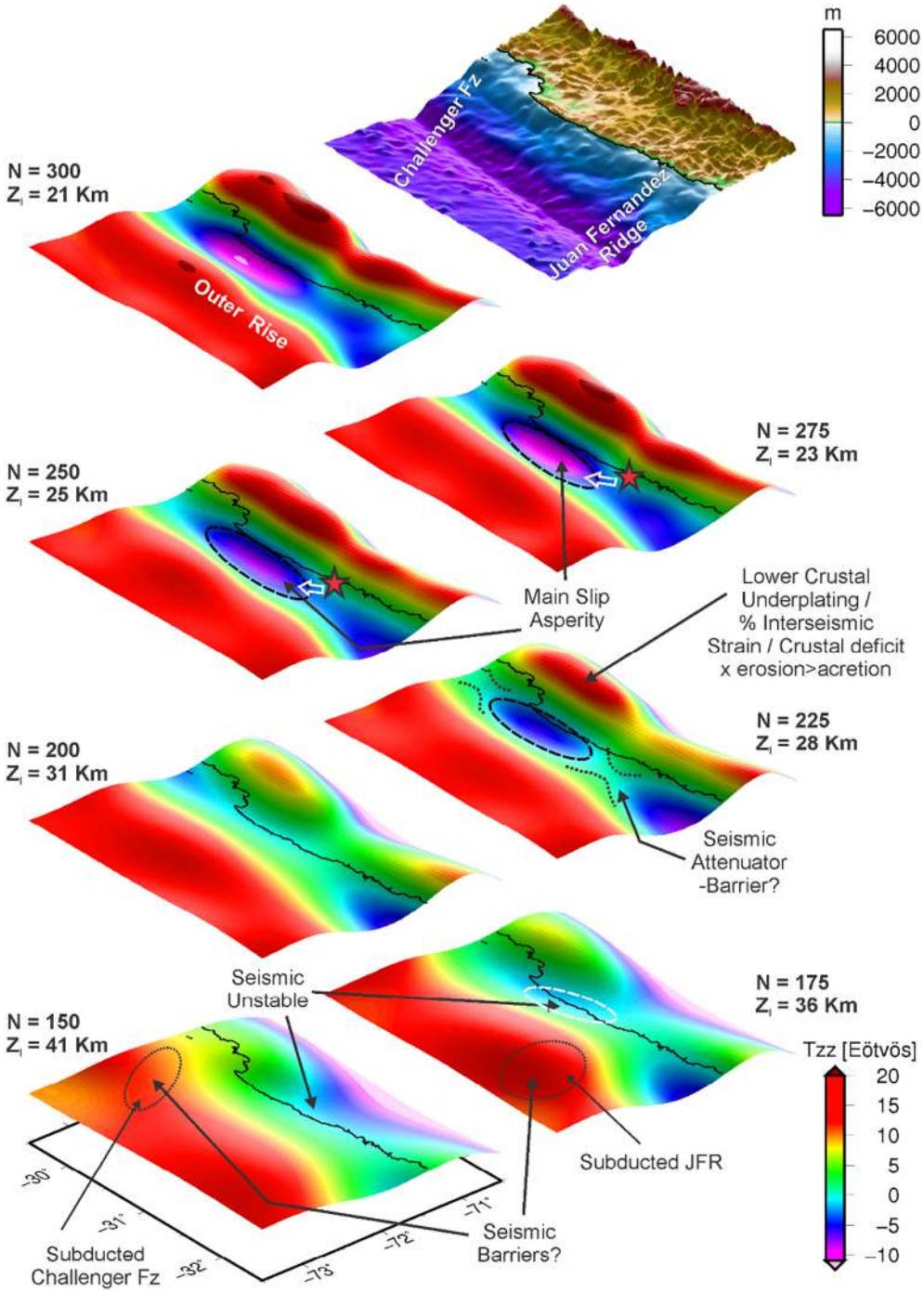
m
6000
4000
2000
0
−2000
−4000
−6000
Challenger Fz
Juan Fernandez Ridge
N = 300
Z = 21 Km
Outer Rise
N = 275
Z = 23 Km
N = 250
Z = 25 Km
Main Slip Asperity
Lower Crustal Underplating / % Interseismic Strain / Crustal deficit x erosion>acretion
N = 225
Z = 28 Km
N = 200
Z = 31 Km
Seismic Attenuator -Barrier?
Seismic Unstable
N = 175
Z = 36 Km
N = 150
Z = 41 Km
Tzz [Eötvös]
20
15
10
5
0
−5
−10
Subducted JFR
Seismic Barriers?
Subducted Challenger Fz
−30°
−31°
−32°
−72°
−73°
−71°

Figure 7

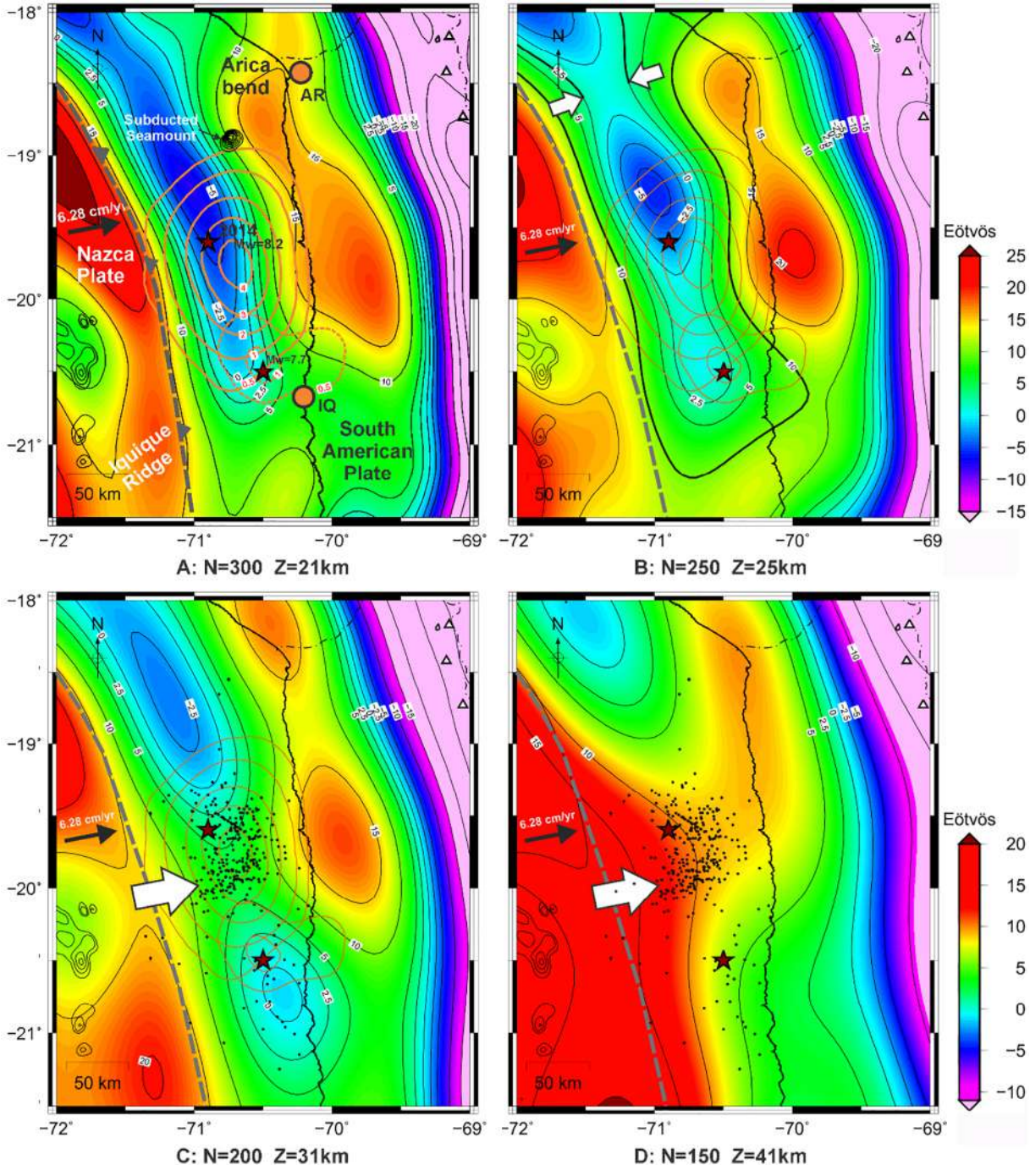
Arica bend
AR
Subducted Seamount
2014 Mw=8.2
Mw=7.7
IQ
Nazca Plate
South American Plate
Iquique Ridge
6.28 cm/yr
50 km
Eötvös
A: N=300 Z=21km
B: N=250 Z=25km
C: N=200 Z=31km
D: N=150 Z=41km

Figure 8

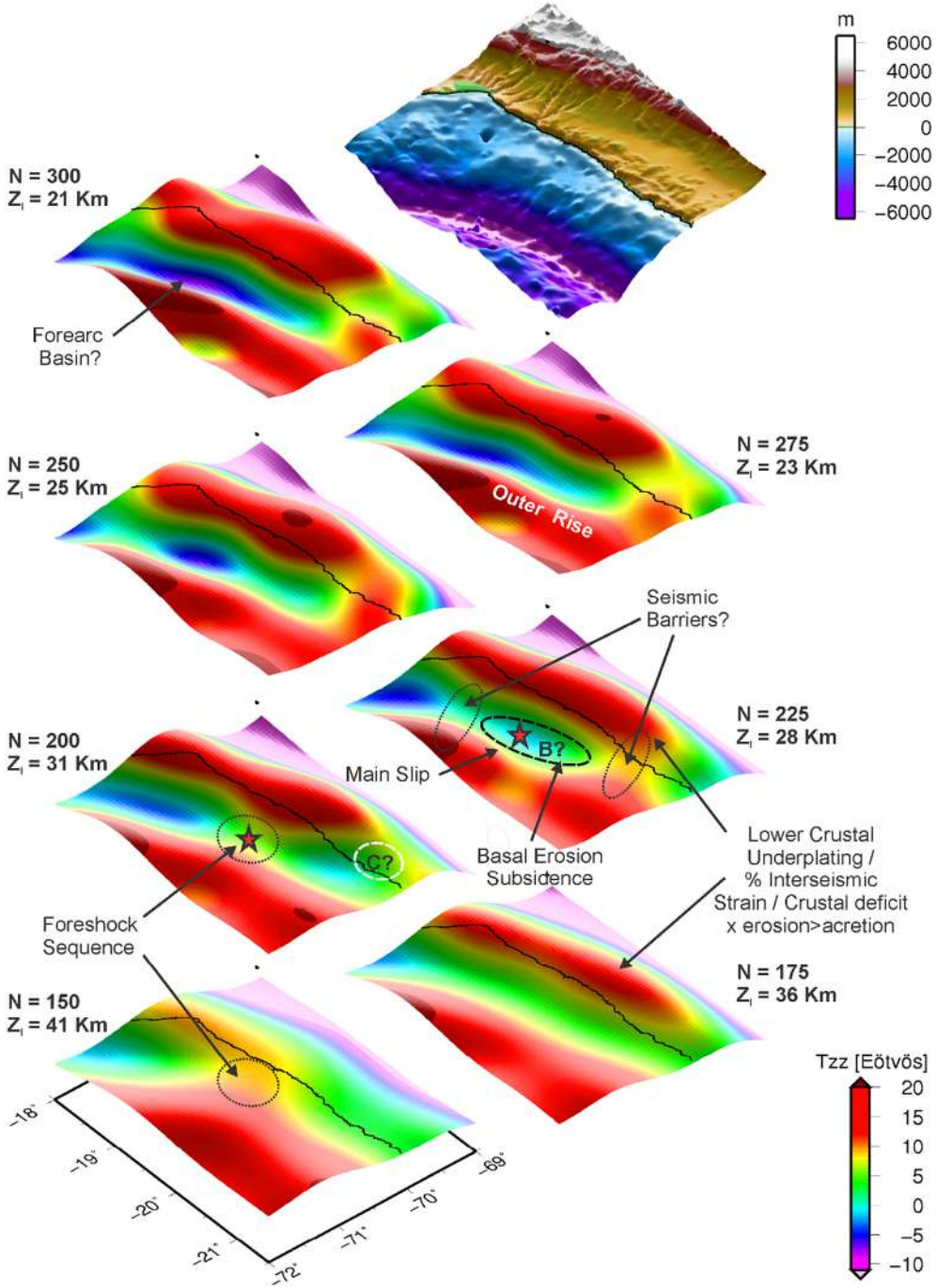
m
6000
4000
2000
0
−2000
−4000
−6000
N = 300
Z = 21 Km
Forearc
Basin?
N = 275
Z = 23 Km
Outer Rise
N = 250
Z = 25 Km
Seismic
Barriers?
N = 225
Z = 28 Km
B?
Main Slip
N = 200
Z = 31 Km
C?
Basal Erosion
Subsidence
Lower Crustal
Underplating /
% Interseismic
Strain / Crustal deficit
x erosion>acretion
Foreshock
Sequence
N = 175
Z = 36 Km
N = 150
Z = 41 Km
−18°
−19°
−20°
−21°
−72°
−71°
−70°
−69°
Tzz [Eötvös]
20
15
10
5
0
−5
−10

Figure 9

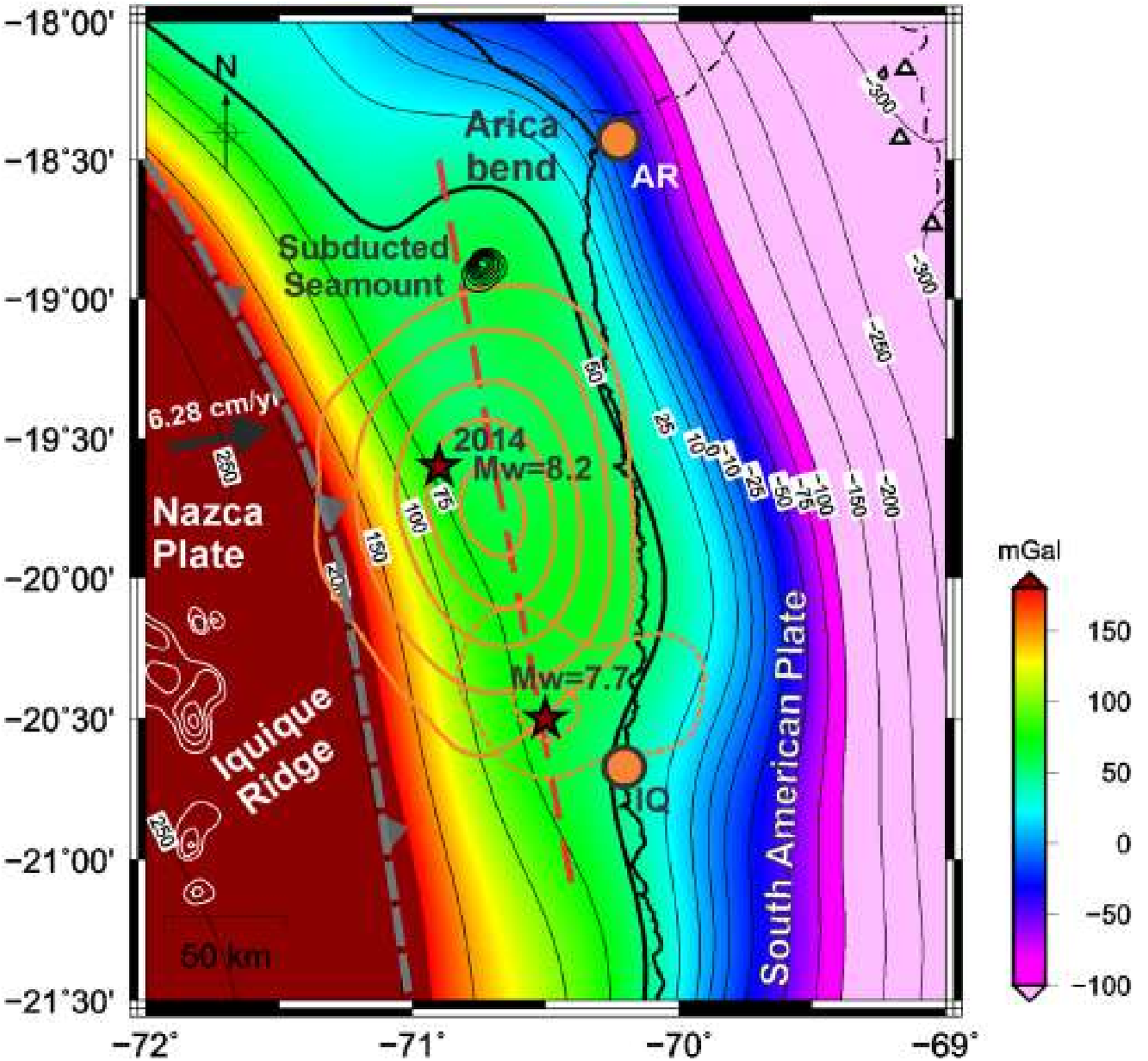
−18˚00'
−18˚30'
−19˚00'
−19˚30'
−20˚00'
−20˚30'
−21˚00'
−21˚30'
−72˚
−71˚
−70˚
−69˚
N
Arica
bend
AR
Subducted
Seamount
2014
Mw=8.2
Mw=7.7
6.28 cm/yr
Nazca
Plate
South American Plate
Iquique
Ridge
IQ
50 km
mGal
150
100
50
0
−50
−100

Figure 10

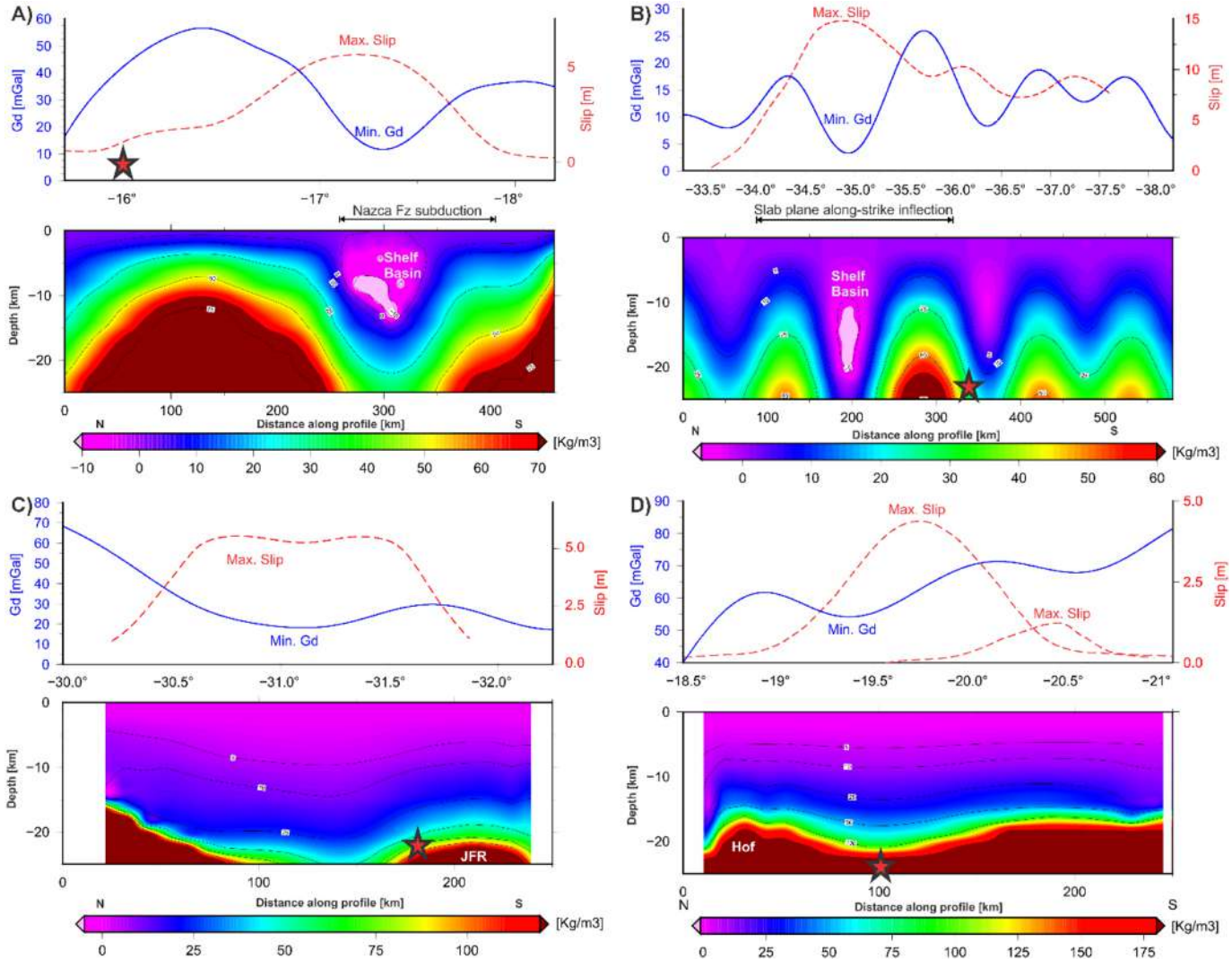
A)
Gd [mGal]
Slip [m]
Max. Slip
Min. Gd
−16°
−17°
−18°
Nazca Fz subduction
Shelf
Basin
Depth [km]
Distance along profile [km]
N
S
[Kg/m3]
B)
Max. Slip
Min. Gd
−33.5°
−34.0°
−34.5°
−35.0°
−35.5°
−36.0°
−36.5°
−37.0°
−37.5°
−38.0°
Slab plane along-strike inflection
Shelf
Basin
C)
Max. Slip
Min. Gd
−30.0°
−30.5°
−31.0°
−31.5°
−32.0°
JFR
D)
Max. Slip
Min. Gd
Max. Slip
−18.5°
−19°
−19.5°
−20.0°
−20.5°
−21°
Hof

Figure 11

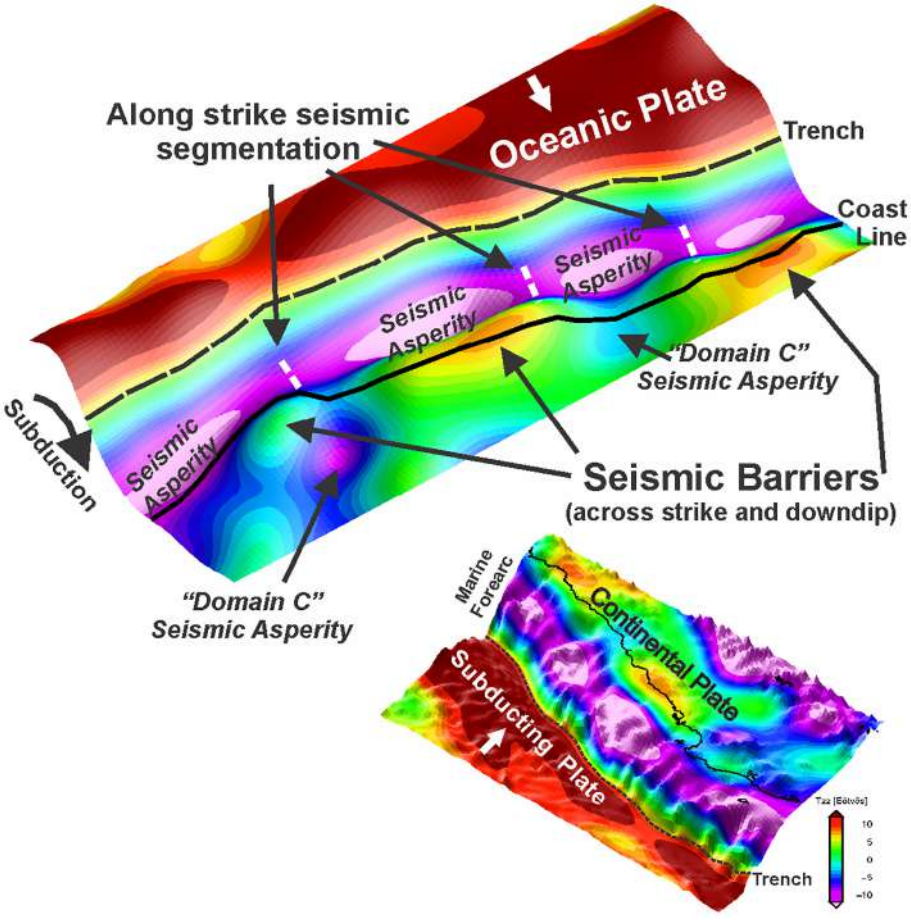
Along strike seismic segmentation
Oceanic Plate
Trench
Coast Line
Seismic Asperity
Seismic Asperity
Seismic Asperity
"Domain C" Seismic Asperity
Subduction
Seismic Asperity
Seismic Barriers
(across strike and downdip)
"Domain C" Seismic Asperity
Marine Forearc
Continental Plate
Subducting Plate
Trench
10
5
0
-5
-10

Figure 12